THERMAL CHARACTERISTICS OF THE ROOSEVELT HOT SPRINGS SYSTEM, WITH FOCUS ON THE FORGE EGS SITE, MILFORD, UTAH

by Rick Allis[1], Mark Gwynn[1], Christian Hardwick[1], Will Hurlbut[1], Stefan M. Kirby[1], and Joseph N. Moore[2]

[1]Utah Geological Survey, Salt Lake City, Utah
[2]Energy & Geoscience Institute, University of Utah, Salt Lake City, Utah

Miscellaneous Publication 169-D
Utah Geological Survey
a division of
UTAH DEPARTMENT OF NATURAL RESOURCES

This paper is part of *Geothermal Characteristics of the Roosevelt Hot Springs System and Adjacent FORGE EGS Site, Milford, Utah*. https://doi.org/10.34191/MP-169

Bibliographic citation:

Allis, R., Gwynn, M., Hardwick, C., Hurlbut, W., Kirby, S.M., and Moore, J.N., 2019, Thermal characteristics of the Roosevelt Hot Springs system, with focus on the FORGE EGS site, Milford, Utah, *in* Allis, R., and Moore, J.N., editors, Geothermal characteristics of the Roosevelt Hot Springs system and adjacent FORGE EGS site, Milford, Utah: Utah Geological Survey Miscellaneous Publication 169-D, 22 p., https://doi.org/10.34191/MP-169-D.

THERMAL CHARACTERISTICS OF THE ROOSEVELT HOT SPRINGS SYSTEM, WITH FOCUS ON THE FORGE EGS SITE, MILFORD, UTAH

by Rick Allis, Mark Gwynn, Christian Hardwick, Will Hurlbut, Stefan M. Kirby and Joseph N. Moore

ABSTRACT

The heat loss from the Roosevelt Hot Springs (RHS) system is 60–70 MW and is predominantly due to the subsurface outflow of about 60 kg/s of hot groundwater from the northern Opal Mound fault (OMF). Prior to development for geothermal power, the main surface feature was a spring close to boiling with a flow rate of 1 kg/s and a heat output of less than 500 kW. The formation of a steam zone in the reservoir due to development has caused steaming ground to replace the hot spring, and the heat loss is now about 10 MW. The high-temperature outflow to the northwest has a prominent temperature inversion below 300 m depth indicating it has been present for 100–1000 years. There is a lower-temperature outflow from the central and southern OMF that has no temperature inversion and a gradient in alluvium below the water level of about 70°C/km. This gradient is indicative of the underlying conductive heat flow and implies the outflow has been present for at least several tens of thousands of years. This southern outflow is occurring from 1–2 km north of Opal Mound up to 5 km south of the Mound. The Opal Mound and sinter deposits farther north adjacent to the OMF may have built up during periods of higher pressure in the evolution of the RHS system, perhaps during the highstand of Lake Bonneville 18,000 years ago.

The Frontier Observatory for Research in Geothermal Energy (FORGE) Milford site is situated over the flank of a granitic intrusion that outcrops to the east in the Mineral Mountains and has a temperature of more than 200°C at 2.4 km depth directly beneath the site. Integration of the thermal data from over 100 thermal gradient and deep exploration wells suggests that about 70 km^2 of the intrusion has a temperature of at least 200°C at 3 km depth. The temperature profile from the 2.3-km-deep well 58-32 that was drilled for the FORGE project confirms a predominantly conductive thermal regime within the granite, with the gradient at depth varying between 60° and 90°C/km due to thermal conductivity variations. Measurements of cuttings and core from the well show a wide range of thermal conductivity depending on the composition of the granitic rock. Values vary from 2.0 W/m°C in quartz-poor dioritic rock to 3.9 W/m°C in more quartz-rich granite. These measurements were made at room temperature and need to be reduced by about 15% for the effects of temperature at the 2–3-km-deep FORGE reservoir beneath the site. Integration of thermal conductivity and temperature gradient variations in well 58-32 yields a heat flow of 180 ± 20 mW/m^2. This value appears to be representative of the deep, thermally conductive heat flow in impermeable granite west and east of the RHS hydrothermal system. One-dimensional heat flow models of the conductive thermal regime in two deep wells adjacent to the convective RHS system suggest partial melt could exist below 7–8 km depth.

INTRODUCTION

A review of the thermal characteristics of the Roosevelt Hot Springs (RHS) system was carried out in Phase 1 of the Frontier Observatory for Research in Geothermal Energy (FORGE) project, with a summary presented by Allis et al. (2015). This review expanded the original assessment of the heat flow at RHS by Ward et al. (1978) by adding other thermal data from exploration wells drilled after 1978. The initial state and response of the Blundell borefield to production and injection was analyzed by Allis and Larsen (2012), and an update of the fluid chemistry characteristics and changes has been reviewed by Simmons et al. (2018; in preparation).

The near-surface thermal characteristics of the RHS are delineated by the temperatures at 200 m depth obtained from more than 50 thermal gradient wells drilled mostly in the late 1970s (Figure 1). The highest temperatures (> 80°C) occur over the top of the hydrothermal system on the east side of the Opal Mound fault (OMF), and this area is tapped by the Blundell geothermal power plant production wells. Temperatures at greater depth here are close to boiling-point for depth over the upper few hundred meters and the profile is near-isothermal below about 400 m depth. These wells tap what is often called the upflow zone. The northwest extension of the high-temperature zone at 200 m depth is due to an outflow of hot groundwater. The 80°C isotherm at 200 m depth is approximately equivalent to a heat flow of 1000 mW/m^2. When integrated across the entire RHS system, the total heat output is 60–70 MW. Assuming a temperature of 270°C (enthalpy of 1180 kJ/kg) in the deep upflow zone of the hydrothermal system, the pre-development mass flow of the system was 60 kg/s.

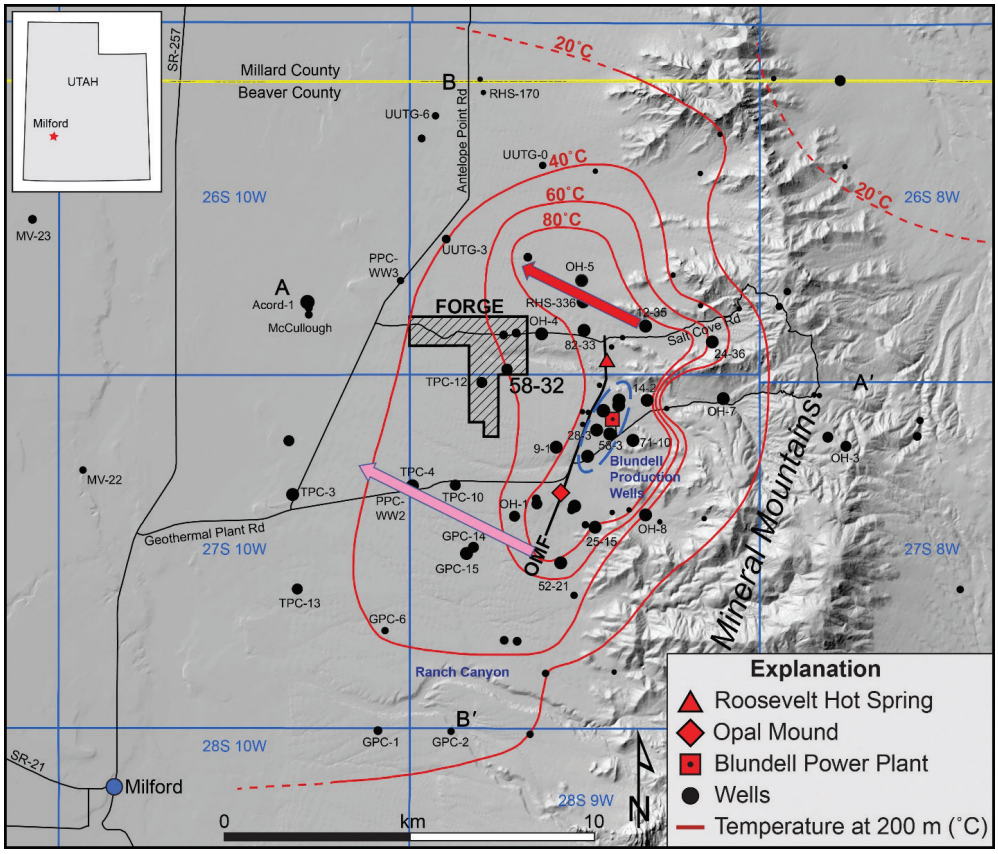

Figure 1. *Thermal regime at 200 m depth. The degree of certainty of the thermal data is indicated by the size of the dot for the well location (all wells are deeper than 50 m). The largest size is for wells greater than 200 m depth where the temperature was observed. The smallest size is for wells about 50 m deep where the temperature had to be extrapolated to a much greater depth and the temperature is considered the least certain. On the east side of the thermal anomaly, the contours represent the temperature at 200 m below the 1830 m above sea level (6000 ft asl) datum, which is the elevation of the alluvial fan near to where it laps against the Mineral Mountains. The 1830 m asl datum allows the contours beneath the flanks of the Mineral Mountains to be smoothed across the ridges and valleys, but requires that higher-elevation wells be extrapolated to greater depths (up to 405 m from the surface). West of the OMF the contours are 200 m below the surface, and near SR-257 in the middle of the valley this is at about 1325 m asl (4345 ft asl; ground surface about 5000 ft asl or 1525 m asl). See Figure 18 for cross sections A–A′ and B–B′. Red and pink arrows indicate relatively young (red, ~ 1000 y) and long-lived (pink, ~ 10,000 y) outflows of geothermal groundwater.*

SURFACE THERMAL ANOMALIES

Roosevelt Hot Springs is located near the northern end of the OMF and was the only thermal feature recorded in the area prior to exploration and development of the hydrothermal system (Lee, 1908; Ward et al., 1978; Capuano and Cole, 1982). In the late 1800s and early 1900s the hot springs became a resort with a bathhouse and other facilities, and the water was used for medicinal purposes. Lee (1908) suggests a flow of at least 1 L/s (about 1 kg/s) of boiling water "strongly charged with hydrogen sulphide." The last high-temperature sample collected at the spring was in 1950 (85°C; Mundorff, 1970). By the time exploration was occurring in the 1970s, the spring had become a warm seep, but had similar chemistry to the 1950 analysis. Although there are hot spring deposits along at least a 5 km length of the OMF (Nielson et al., 1986; Kirby et al., 2018), there were no reports of associated thermal ground or seeps before development. The heat loss from the original hot spring assuming the flow rate and boiling temperature in Lee (1908) was about 300 kW, a tiny fraction of the subsurface heat output being carried by the underlying hot groundwater.

Informal comments from the operators of the Blundell power plant indicate an expansion of thermal ground occurred during the mid-1980s after the power plant was commissioned. This expansion is corroborated by comparison of aerial photos of the RHS area pre-development and more recently (Figure 2). Areas of steam-heated ground expanded, junipers and grasses died off, and areas of bare ground expanded. However, the 1955 photo shows that there was a lack of junipers in areas that subsequently became steam-heated. Growth here may have been restricted by a subtle gas flux from depth or intense hydrothermal alteration.

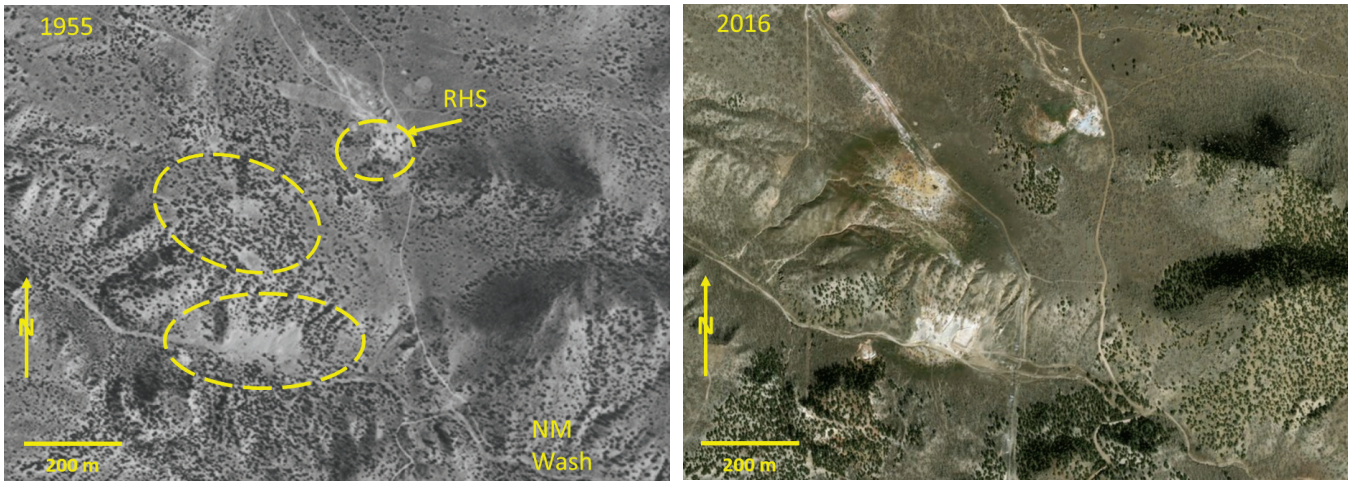

Figure 2. *Historical comparison of the vegetation patterns and thermal features around Roosevelt Hot Springs (1955 and 2016 imagery). Development of the hydrothermal system for power caused an increase in steam-heated ground and a die-off of vegetation. A major fire in 2007 (Milford Flat fire) burned much of the vegetation, so caution is required interpreting the changes. NM Wash is the Negro Mag Wash. Yellow dashed ellipses on the 1955 photo outline the areas of future steam-heated ground.*

The intensity and size of the thermal anomalies were measured in the spring of 2012 using a 20-cm dial-type thermometer (Figure 3). Measurements at different times of the day and on different days were compared to temperatures at several base stations on non-thermal ground and were adjusted to anomalies above ambient. The accuracy of the anomalies is estimated to be ±2°C. Three distinct areas have thermal ground: north of Negro Mag Wash (including the original RHS), adjacent to production well 28-3 in the production well field, and on part of the Opal Mound. A pressure decline due to production has caused a steam zone to form over the hot liquid reservoir, and steam is leaking to the surface (Allis and Larsen, 2012). A detailed assessment of the heat loss from the steaming ground has not been attempted, but a rough comparison of typical heat loss rates and the area of steaming ground elsewhere (Allis et al., 1999; Bromley at al., 2011) suggests that surface heat loss has increased to about 10 MW.

THERMAL GROUNDWATER REGIME

At 200 m depth, for a typical conductive Great Basin heat flow of 90 mW/m^2 and an average surface temperature of 12°C, the temperature should be about 24°C and the gradient in the overlying unconsolidated sediment should be about 60°C/km (assuming a thermal conductivity of 1.5 W/m°C). In low-porosity crystalline rocks (thermal conductivity of about 3 W/m°C), the equivalent temperature is about 18°C and the gradient is about 30°C/km. In the Mineral Mountains where the crystalline rocks outcrop, the elevation rises over a kilometer above the valley floor, so the mean annual surface temperature could be 5°–10°C cooler due to the adiabatic lapse rate in the atmosphere. The temperature at 200 m depth near the ridge of the Mineral Mountains, assuming thermal conduction from the surface and 90 mW/m^2, implies an ambient temperature of about 13°–15°C. Temperatures at 200 m depth greater than about 30°C in the valley, and greater than about 20°C in the Mineral Mountains, are therefore anomalously warm. Examples of thermal gradients are shown in Figure 4.

When the thermal gradient data for the central, southern, and western sectors are plotted against depth, the near-surface profiles (less than about 80 m depth) are surprisingly similar. The gradient of 270°C/km is equivalent to a heat flow of 400–500 mW/m^2 (average thermal conductivity of 1.5–1.7 W/m°C). The thermal gradients decrease by almost a factor of four at greater depth, which Wilson and Chapman (1980) attribute to a corresponding increase in thermal conductivity at the transition to water-saturated rock. If this is correct, then all wells should show the same effect at the water table. Because several wells show no change in thermal gradient at the water table (e.g., OH4, OH5, GPC15), it seems more likely that some other factor such as a cross flow of warm water at the water table may be causing this gradient change at the water table. In addition, several wells in the central part of the valley exhibit a uniform thermal gradient from the ground surface through the water table consistent with the zero-depth intercept being close to the mean annual temperature (for example, MV22, 23, McCullough). There is no evidence of cross-flowing warm water in these three wells, and they may reflect the undisturbed regional thermal regime (discussed in more detail in the Regional Heat Flow section).

When all the temperature profiles in gradient wells are plotted against elevation, the profiles are spread from warmer in the east (GPC-15) to cooler in the west (for example, TPC-3 near the intersection of Geothermal Plant Rd. and Antelope Pt. Rd.). The

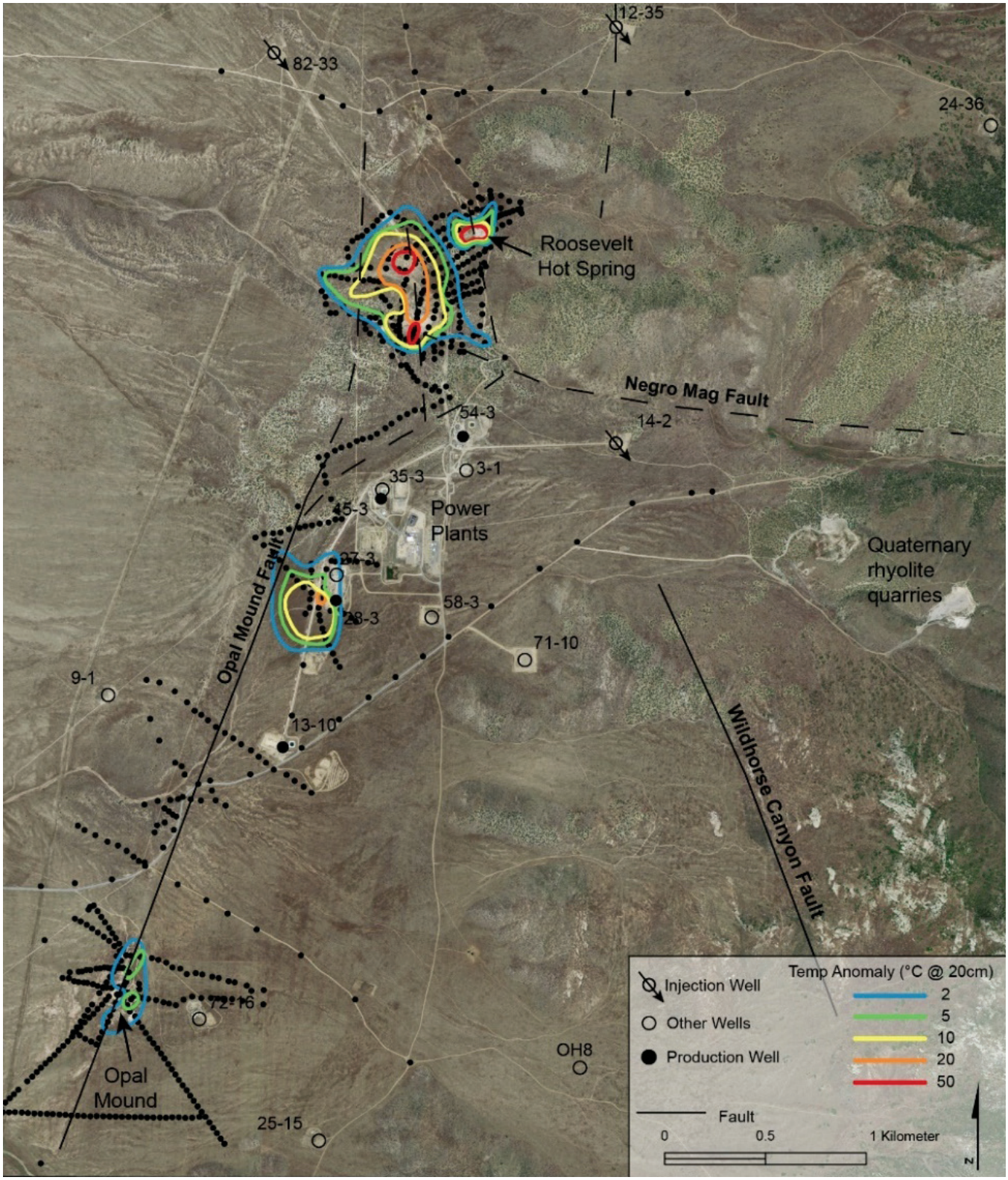

Figure 3. *Temperature anomalies at 20 cm depth (°C above ambient; small dots are measurement points) adjacent to the OMF in 2012. Well 71-10 became an injection well in 2016 and well 58-3 became a production well in 2018.*

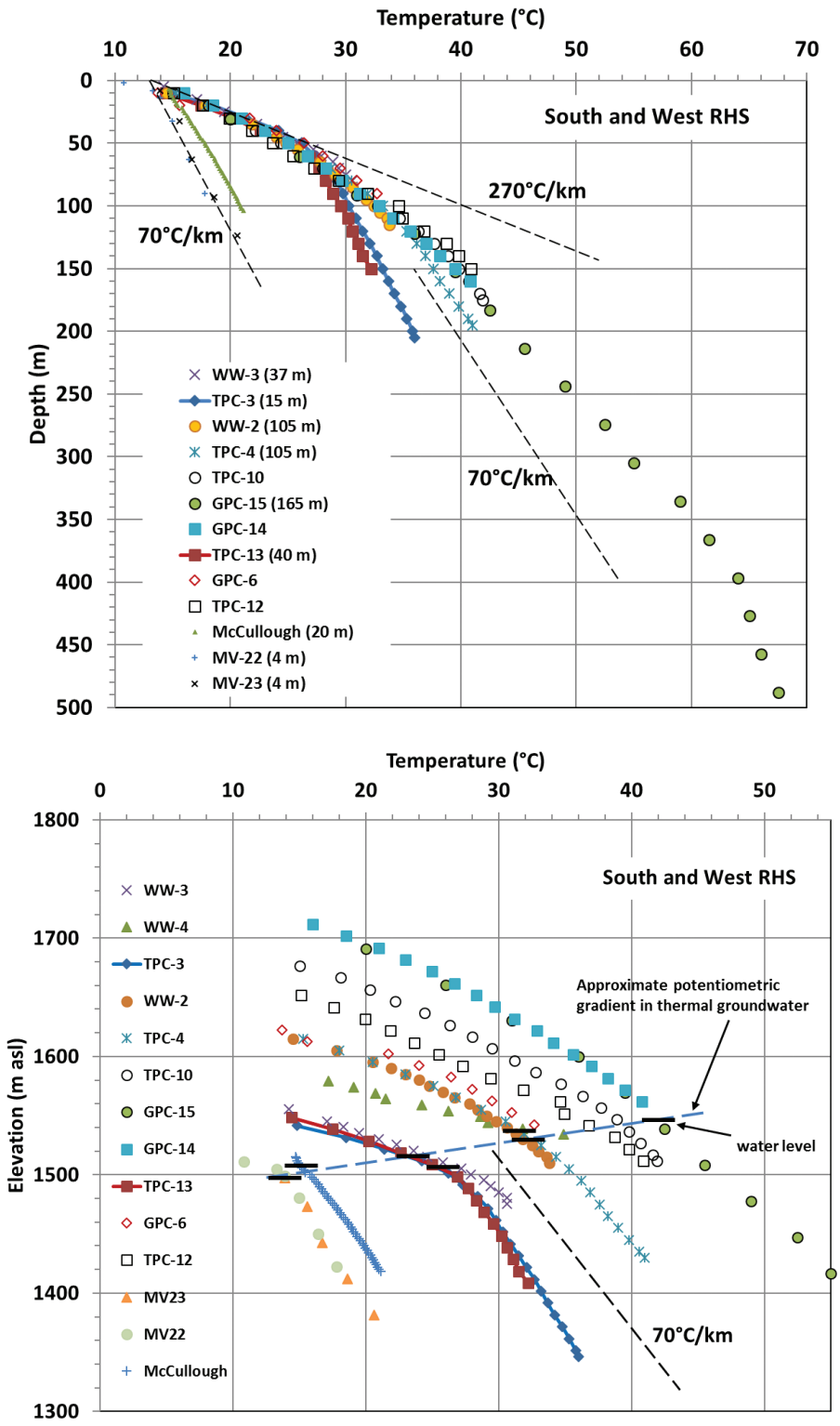

Figure 4. *Upper: Temperature profiles from thermal gradient wells around the southern and western areas of the RHS system, plotted against depth below the ground surface. Although most wells over the RHS system have shallow temperature gradients exceeding 200°C/km, the deeper thermal gradients are 70°C/km (water level in brackets, either from measurements in that well, or from a nearby well and documented by Kirby et al. [2019]). Lower: Temperature plotted against elevation (meters above sea level) shows a pattern of warm groundwater flowing from east to west, with the high thermal gradients at shallow depth in the vadose zone, and apparently conductive thermal profiles below and above the water table.*

water levels also decrease in elevation from east to west, confirming an outflow of warm groundwater (50 m of head change over 10 km; Kirby et al., 2019). The temperature of the outflow at the water table decreases from 42°C in GPC-15, to 25°C in TPC-3. This cooling of the groundwater appears to be due to both conductive heat flow through the vadose zone and mixing with infiltrating meteoric water (evidence of dilution towards the west; Kirby et al., 2019).

In the northern sector of RHS, where the northwest-directed plume flows from the northern end of the OMF, there is evidence of hot water outflow between 1300 and 1500 m asl. Well OH-5 best captures the character of the outflow plume (Figure 5). The new FORGE well 58-32 is suspected to be near the west edge of this plume, with the thermal profile suggesting a lateral flow at 40° to 45°C between 1300 and 1500 m asl. The temperature of the source of the plume probably exceeds 130°C based on the temperature in well 82-33 and may be about 200°C where it flows from the northern end of the OMF (well 12-35).

The pattern of a warm outflow in south-central RHS with an underlying uniform temperature gradient, contrasts with the inversion present beneath the hot outflow in northern RHS. The change in gradient is a phenomenon that was studied by Ziagos and Blackwell (1981, 1986). They showed that the thermal effect of a horizontal outflow of warm groundwater initially causes a temperature inversion beneath the outflow, but after a long time of continued warm outflow the underlying thermal regime heats up to reflect the regional equilibrium thermal gradient (Figure 6). The time frame for the inversion to disappear is tens of thousands of years. This type of thermal signature was used to interpret that a lateral flow of hot water on top of the Precambrian basement beneath the Fenton Hill hot dry-rock test site had been occurring for about 10,000 years (Harrison et al., 1986). A long-lived thermal outflow may help explain the fossil siliceous sinter at Opal Mound near the southern end of the OMF in contrast to the recent active hot spring area at the northern end of the OMF. Although the sinter at Opal Mound exhibits a transition from Opal-A to diagenetic quartz, and in New Zealand this transition takes about 40,000 years, the two dates from the Opal Mound are between 1000 and 2000 years (Lynne et al., 2005). Perhaps the core of the Opal Mound is significantly older than the two dates imply. In contrast, based on the thermal inversion, the hot groundwater plume northwest of the RHS maybe be relatively young (~ 1000 years). The deepest well in the south-central RHS west of the OMF, GPC-15 (580 m deep), has a second decrease in temperature gradient below 400 m depth which may be evidence of decreasing temperature with time of this long-lived thermal outflow.

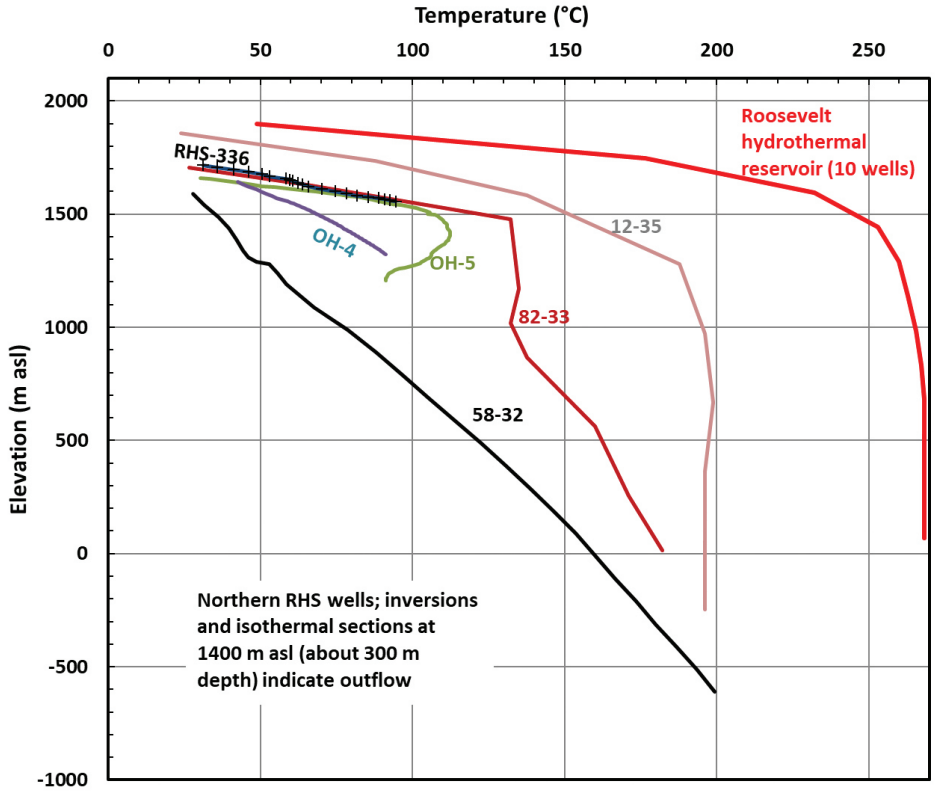

Figure 5. *Temperature profiles in wells around the northwest part of the RHS system near the main outflow zone of hot water. The outflow is characterized by temperature inversions (OH-5) and isothermal zones between 1500 and 1300 m asl (typically 200–400 m depth). FORGE well 58-32 appears to be outside the hot outflow but does show anomalously cooler conditions suggestive of lateral groundwater flow in this depth range.*

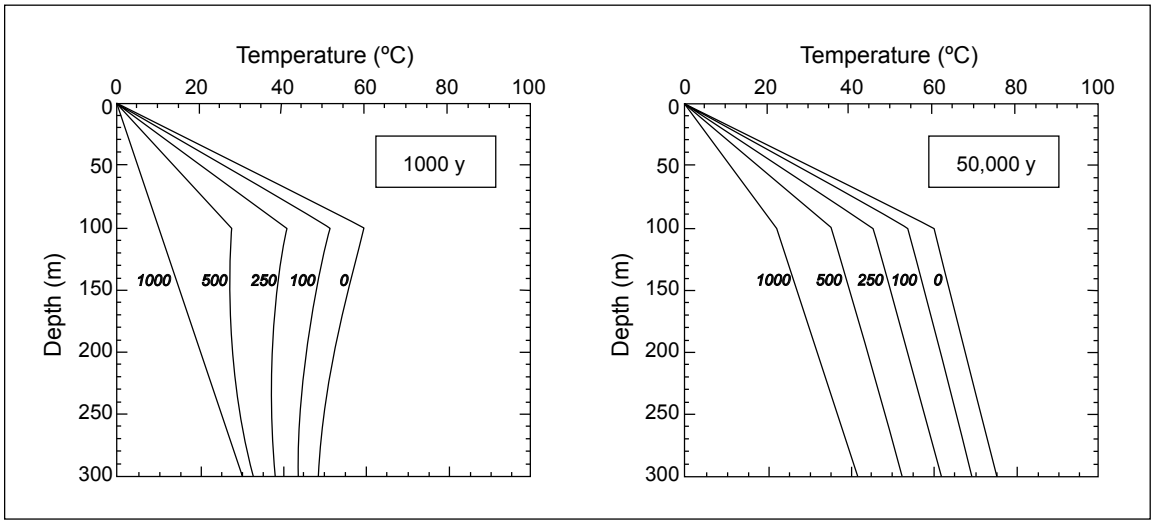

Figure 6. *Theoretical temperature-depth profiles for the thermal effects due to lateral flow in an aquifer at 100 m depth at 60°C at the recharge point (0 m) and at distances up to 1000 m from the recharge point (water flow rate of 1 m/year assumed; 100°C/km ambient gradient). On a scale of hundreds to thousands of years, there is a temperature inversion beneath the aquifer; on a scale of tens of thousands of years, the thermal regime at depth is the equilibrium gradient (Ziagos and Blackwell, 1981, 1986).*

REGIONAL THERMAL REGIME

As discussed in the previous section, the temperature gradient in the groundwater west of the OMF has a characteristic value of about 70°C/km, although over a large area the gradient is displaced to higher temperatures (Figure 4). In the Mineral Mountains east of the RHS thermal anomaly the profiles in exploration wells typically show low thermal gradients (10°–20°C/km) which extrapolate to zero-depth temperature intercepts of 8°–10°C. These low gradients are consistent with the effects of downward percolation of meteoric water into the mountainous terrain. The deepest well near the ridgeline of the Mineral Mountains (OH-3, Figure 1) is 660 m deep and has a gradient of 21°C/km (Forrest, 1994).

West of the obvious thermal groundwater anomaly in north Milford Valley several temperature gradient wells have zero-depth temperature intercepts similar to the mean annual ground-surface temperature for the elevation (13° ± 2°C) and have a gradient of 60° ± 5°C/km (Figure 7). Assuming a thermal conductivity for the basin fill of 1.5 W/m°C implies a heat flow of 90 ± 10 mW/m^2. Uncertainties in thermal conductivity will increase the uncertainties in heat flow.

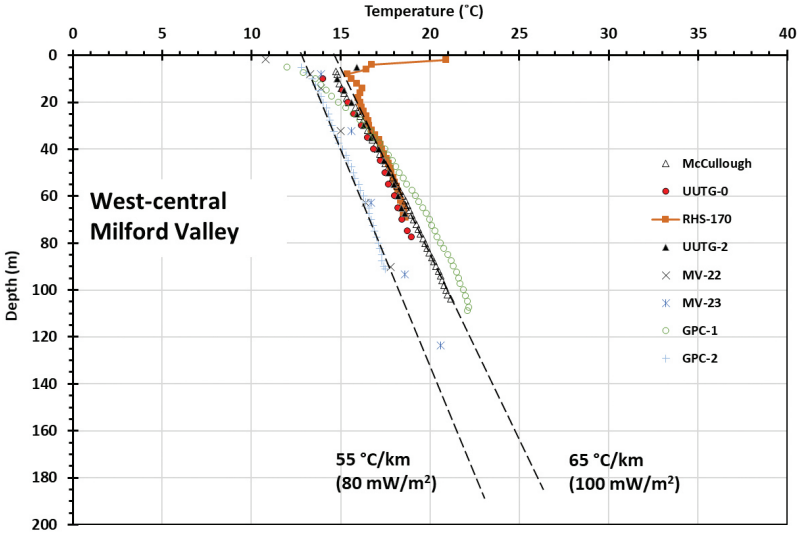

Figure 7. *Temperature profiles in thermal gradient wells in central northern Milford Valley having consistent gradients which extrapolate to the mean annual temperature of the ground surface (13°–15°C). The heat flow values assume an average thermal conductivity for the basin fill of 1.5 W/m°C.*

Acord-1

In 1979 McCullough Oil drilled a well, Acord-1, to 3.5 km depth in the same area as the gradient wells shown in Figure 7. Acord-1 (Figure 1) intercepted granitic basement at 3.0 km depth. Gwynn et al. (2016) analyzed the unusually detailed dataset of bottom-hole temperatures measured as drilling progressed. They showed for reasonable assumptions of thermal conductivity for rock type, a conductive geotherm could fit both the shallow gradient and the corrected bottom-hole temperatures (Figure 8). The heat flow that best fits both the nearby McCullough groundwater temperature profile and the corrected bottom-hole temperatures in Acord-1 is 100 ± 20 mW/m^2. Most of the uncertainty is due to assumptions about thermal conductivity.

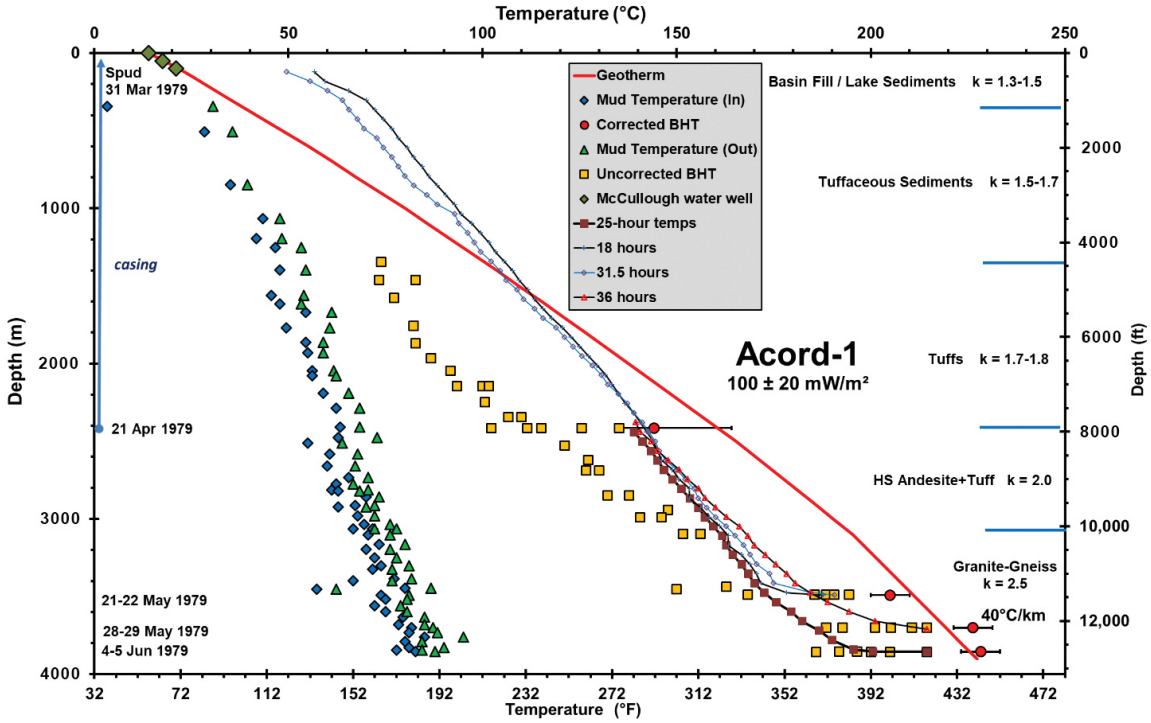

Figure 8. *Temperature data from Acord-1 well during brief stops while the hole was being drilled (Gwynn et al., 2016). The corrected bottom hole temperatures (BHTs) are consistent with a conductive profile, and the best-fit geotherm has a heat flow of 100 ± 20 mW/m^2 (uncertainty due to thermal conductivity [k; units of W/m°C] assumptions; geotherm fits both the observed shallow thermal gradient at the site and the deep, corrected BHTs). The temperature gradient in the granite is 40°C/km.*

Deep Wells Near the RHS Wellfield

Numerous deep exploration wells were drilled around the RHS system before the most productive zone (sometimes referred to as the "reservoir") for geothermal power generation was identified. Equilibrium profiles for these wells are shown in Figure 9 (locations on Figure 1). Wells tapping the hydrothermal reservoir are distinctive because of their high near-surface temperature gradient (typically close to a boiling point-for-depth profile) and near-isothermal zone below about 500 m depth. The near-isothermal conditions in the reservoir are consistent with the upflow of fluid at more than 265°C (Ward et al., 1978; Faulder, 1991, 1994; Allis and Larsen, 2012; Simmons et al., 2015, in preparation). Most wells outside the upflow zone are much cooler near-surface but have constant temperature gradients below about 1 km depth which can be extrapolated to greater depth. This contrast is indicative of poor permeability, lack of fluid flow, and thermal conduction as the dominant form of heat transfer. The new well drilled for the FORGE project, 58-32, is similar, with a deep gradient between 60° and 90°C/km below 800 m depth (discussed in next section). Most of these wells point to temperatures of more than 250°C at depths of 3–4 km. These deeper wells provide proxies for extrapolating nearby thermal gradient wells and enable isotherm maps to be compiled at different depths (described in a later section).

FORGE Well 58-32

FORGE well 58-32 was completed in October 2017 after two months of drilling and subsequent testing (Moore et al., 2018). Because of the volume of thermal data available, its thermal regime is discussed here in detail. Precision temperature and

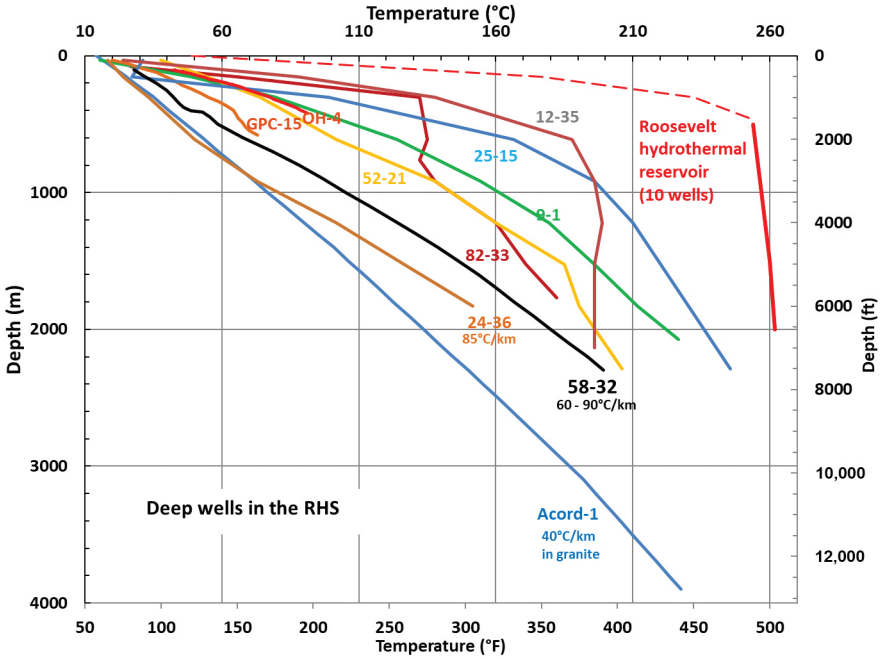

Figure 9. *Temperature profiles in deep wells mostly drilled during exploration of the RHS hydrothermal reservoir that is now tapped by the Blundell borefield. Within the production borefield, reservoir temperatures prior to development were near boiling point-for-depth, and typically in the range of 255°–265°C at greater depth. Except for well 12-35, which is at the northern end of the reservoir and close to the main outflow zone, and Acord-1, which is near the western edge of the RHS system, the profiles seem to converge on about 250°–270°C at 3–4 km depth.*

pressure profiles were run in the well 37 days after drilling and initial testing had been completed, and 13 months later when it should have been in thermal equilibrium with the host rock (Figure 10). Details of additional thermal measurements made during drilling and attempts to predict the equilibrium rock temperature during a 24-hour stoppage in drilling when the hole was at 2040 m depth are discussed by Allis et al. (2018). In all surveys, the thermal response time of the probe in water was less than 1 second and the temperature accuracy appears to be ± 0.1°C based on the typical logging speed of 15 m/minute (50 ft/minute). The 13-month pressure run showed the water level at 90 m depth, which is at similar elevation to the water level in nearby well OH4 reported by Vuataz and Goff (1987) and Kirby et al. (2019). OH4 bottomed in granite, which suggests that there may be a fracture network connecting 58-32 to the groundwater regime in the granite with sufficient permeability to allow pressure responses within a time-scale of a year.

The 37-day and 13-month logs show that the well cooled over time above 500–600 m depth and heated up below this depth. The temperature pivot of about 60°C corresponds to the typical mud circulation temperature during much of the drilling. The equilibrium temperature profile between 90 and 150 m depth matches the temperature profile in nearby gradient well TPC12, which indicates that the 1980s gradient well data in this part of the RHS system can be used to extrapolate deeper temperatures.

The maximum temperature at the bottom of well 58-32 is 199.4°C (390.8°F). The equilibrium log below about 500 m depth appears to show a conductive thermal profile, but at 90 m and 400 m depth there are jumps in temperature. The 12°C jump at 90 m coincides with the water level in the well and is an artifact of the temperature probe not having time to equilibrate in the air column with the 15 m/minute (50 feet/minute) logging rate. The unexpected thermal feature is the 7°C jump in temperature (46° to 53°C) at 400 m depth. We show below that when a conductive geotherm is fitted to the entire profile, the anomalous zone is characterized by cooler temperatures between 250 and 400 m depth. This coincides with an inversion and local minimum temperature at 300 m depth recorded in the 37-day profile. The anomaly suggests there is some permeability outside the casing and a lateral flow of groundwater between 250 and 400 m depth with a temperature between 40° and 46°C.

The temperature gradient trend with depth (Figure 11) was calculated over a moving 10 m depth interval and plotted at the midpoint. The two depths where the temperature jumped by 7°–12°C have very high gradients and are truncated on the graph. The bedrock interface near 970 m depth shows clearly as an increase in gradient with depth because of the thermal conductivity decrease from compacted granite alluvium to fractured monzodiorite. The thermal conductivity measurements on cuttings every 30 m (100 ft) and corrected to in situ conditions for porosity are shown in Figure 12 (Gwynn et al., 2019). An example of the effect of varying thermal conductivity (due mostly to varying quartz concentration) is the pronounced increase in gradient with depth at 1800 m. The gradient increases downwards from 63°C/km to 70°C/km due to the thermal conductivity decreasing

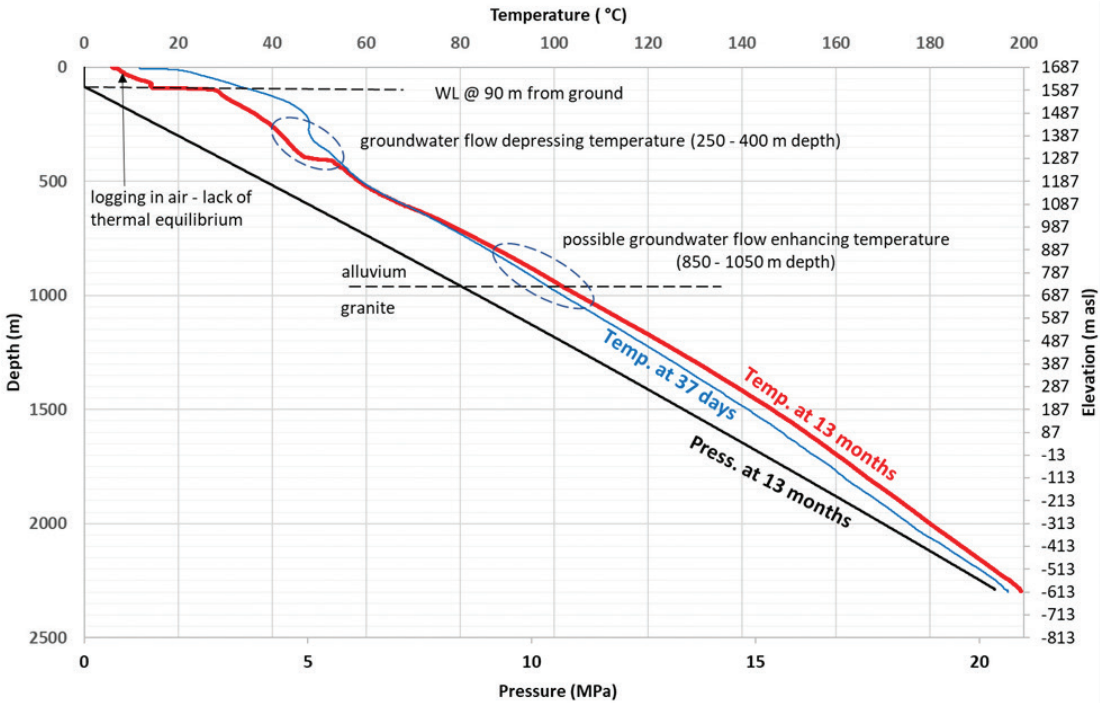

Figure 10. *Temperature profiles from well 58-32 measured on November 2, 2017 (blue line), and November 8, 2018 (red line). WL is water level in the well during the November 8 survey. During the November 2 survey the water level was about 1 m from the ground level (1687 m above sea level [asl]). The pressure profile measured on November 8 is shown as the black line. Dashed ellipses identify zones that do not fit a 1-D conductive geotherm.*

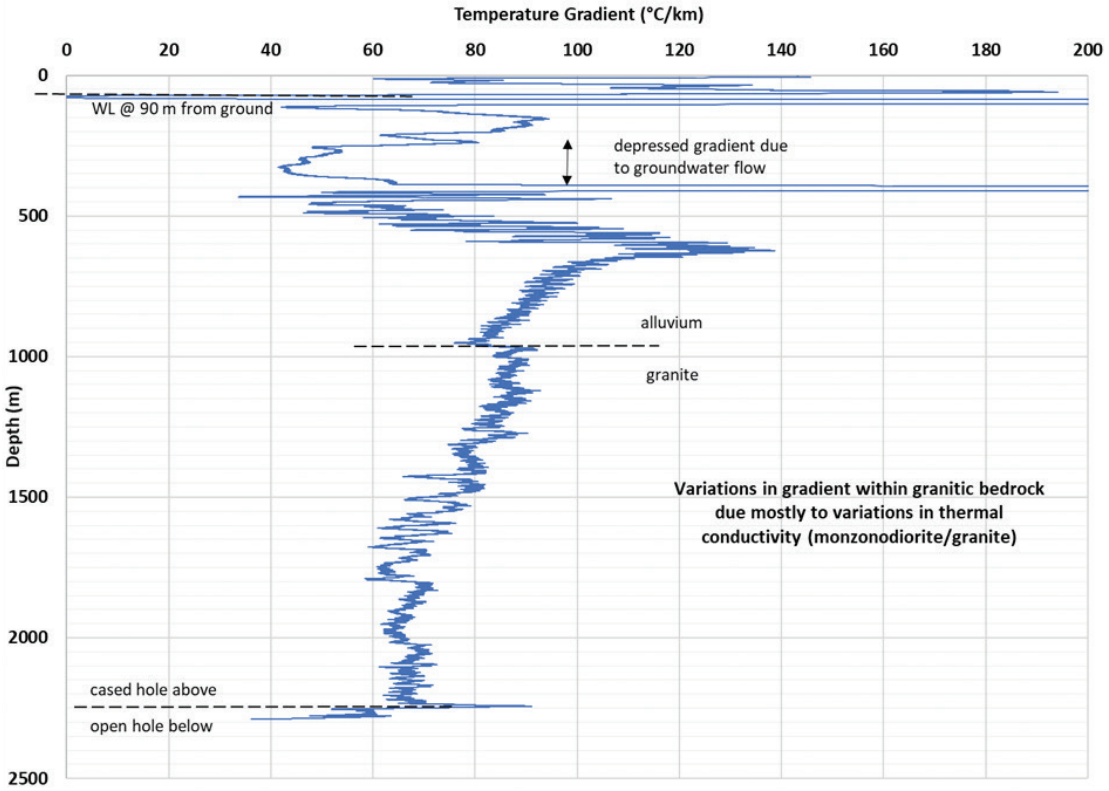

Figure 11. *Variation in temperature gradient with depth calculated from the temperature profile based on a moving average over 10 m.*

from just over 3.5 to just under 2.5 W/m°C at that depth (Figures 11 and 12). The temperature gradient variations within the bedrock appear to be largely due to thermal conductivity effects. Gwynn et al. (2019) note from both outcrop examples and from the wireline logs in 58-32 that lithologic variations in the bedrock ranged from centimeter-scale veins, up to more than 100 m in scale with mappable geologic units. The 30 m spacing of thermal conductivity measurements on cuttings is too coarse to allow direct correlation of temperature gradient and conductivity.

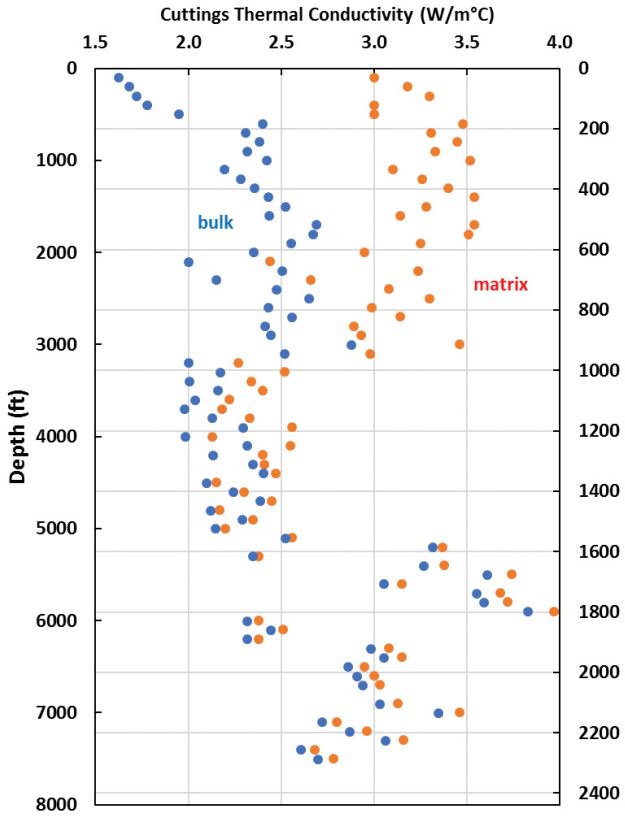

Figure 12. *Thermal conductivity data for well 58-32 based on cuttings measurements using a divided bar. Matrix thermal conductivity values are corrected for the effects of rock porosity using the wireline geophysical logs (formation density log; Gwynn et al., 2019). The variation in thermal conductivity is largely due to the quartz content of the rock. The transition from granitic basin fill to granitic bedrock occurs at 970 m.*

The temperature gradient within the granitic bedrock varies between 60° and 90°C/km and has a general trend of gradually decreasing gradient with increasing depth. The bedrock thermal conductivity (Figure 12) shows the opposite general trend increasing from 2.2 ± 0.2 W/m°C above 1600 m depth to 3.1 ± 0.6 W/m°C below 1600 m depth. One way of integrating the conductivity and gradient variations is to derive a thermal resistance plot (Bullard, 1939). The Fourier equation for conductive heat transport can be rearranged so that a temperature versus thermal resistance plot yields a line whose slope is the conductive heat flow:

$$\Delta T_i = Q * \Delta z_i / k_i ,$$

where T_i is the temperature at depth increment z_i with thermal conductivity k_i, and Q is the conductive heat flow. This plot allows departures from a uniform conductive heat flow to be highlighted. The thermal resistance plot for 58-32 using the thermal conductivity data at 30 m intervals is shown in Figure 13.

Figure 13 indicates a heat flow of 200 mW/m^2 and has an intercept of 13°C, which is similar to the mean annual ground temperature for the region, and points to a long-lived (10^4–10^5 years) thermal regime. Three zones on the plot suggest departures from uniform conductive heat flow. Temperatures are anomalously low above the water level due to the lack of thermal equilibrium from logging in air; temperatures are also several degrees low at 250–400 m depth; and there is a broader depth zone centered near the alluvium/bedrock interface where temperatures are a few degrees higher than the uniform heat flow trend. Assuming the two anomalous zones below the water table are not due to corresponding errors in the thermal conductivity measurements, the simplest explanation for both features is that groundwater flow outside the casing is the cause of the deviations from uniform conductive heat flow. In the case of the anomaly at 250–400 m depth, the thermal feature is also visible in

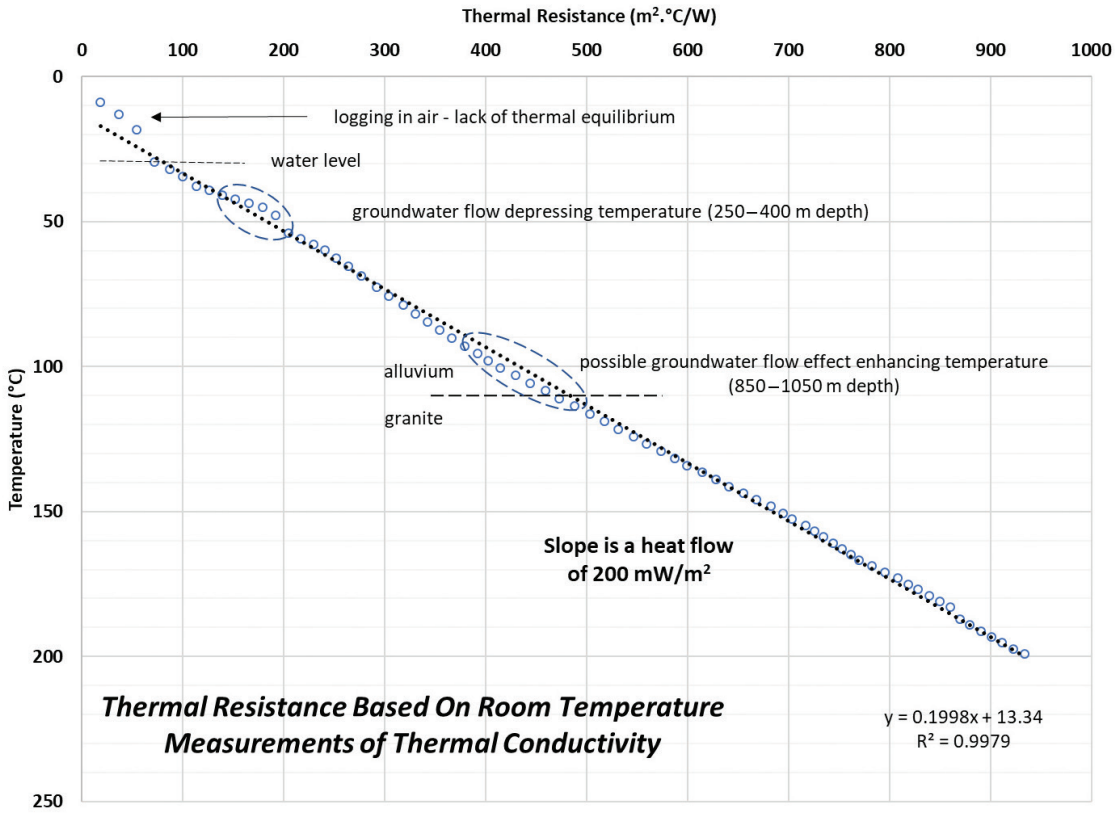

Figure 13. *Thermal resistance-temperature plot for well 58-32. A constant slope on these plots indicates one-dimensional conductive heat flow. In this case the slope is 200 mW/m², using the thermal conductivity measurements derived from the cuttings measurements at room temperature. The location of the water level in the well and the alluvium/granite interface are based on the temperature-depth plot of Figure 10.*

Figures 10 and 11, with its base being the jump in temperature at 400 m depth. The temperatures are up to 5°C too low and based on both the shallow thermal regime shown in Figure 4 and the potentiometric groundwater trend (Kirby et al., 2019), this flow likely to be from the east or south.

The deeper anomaly on the thermal resistance plot (Figure 13) in the temperature range of 90°–110°C (about 850 and 1050 m depth) has temperatures which are warmer than the uniform conductive heat flow trend by up to 5°C. The lowest electrical resistivities recorded in well 58-32 (that is, below top of log at 2200 ft depth) are in a 50 m thick zone at about 1000 m depth below ground level (3300–3400 ft below kelly bushing; resistivity of 5 ohm-meters; Gwynn et al., 2019). This zone is in fractured granitic rock and has the highest concentration of clay (especially illite and kaolinite) observed in the cuttings from the bedrock (Jones et al., 2019). The more intensive alteration here possibly coincides with a lateral flow of hot water which would also cause the relatively wide feature on the thermal resistance plot. It is also possible some lateral flow is occurring in the alluvium just above this clay-rich zone.

Figure 13 ignores the effect of temperature on thermal conductivity, mainly due to the sensitivity of quartz thermal conductivity to temperature. Rock with a higher quartz content has a higher thermal conductivity, but also has a 10%–15% decrease in conductivity between room temperature (about 25°C) and the temperature of 200°C at the bottom of well 58-32. To adjust the thermal resistance plot for this effect, the granitic rock in well 58-32 was assumed to be similar to the Barre granite trend shown in Figure 14. The bulk thermal conductivities in Figure 12 were adjusted based on their original downhole temperature, with the resulting thermal resistance shown in Figure 15. The effect of the temperature correction to thermal conductivity decreases the slope of the best-fit line for FORGE well 58-32 from 200 to 180 mW/m².

SURFACE HEAT FLOW AND ISOTHERM MAPS

The heat flow map, based on numerous thermal gradient wells at less than 200 m depth (Gwynn et al., 2016; Figure 16), delineates the conductive heat loss from the top of the RHS system and its outflow plume. For most wells, gradients were

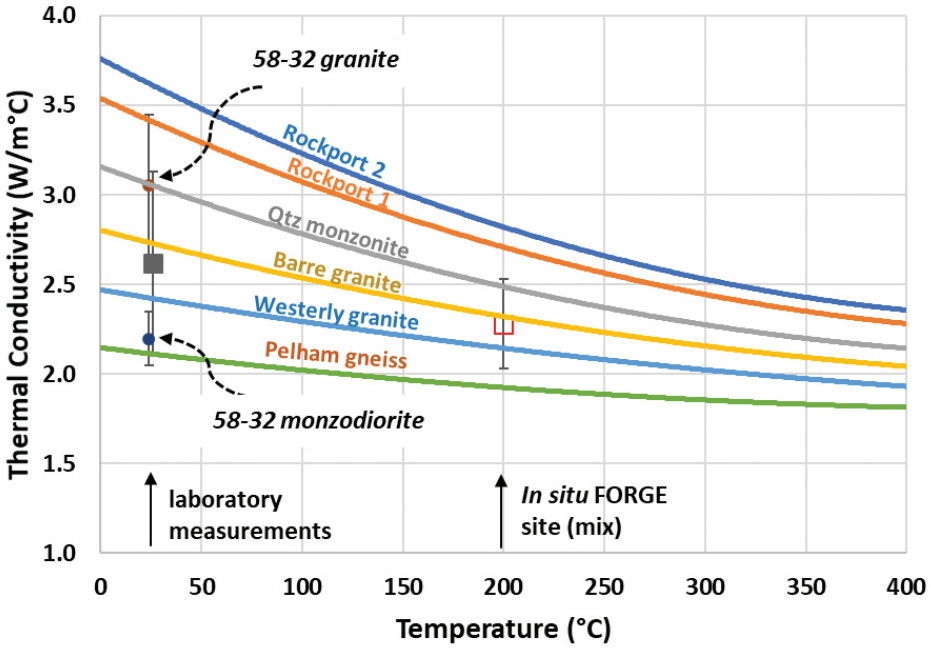

Figure 14. *Variation in thermal conductivity with temperature for granitic rocks from the northeast U.S. (Robertson, 1988). The thermal conductivity for rock in well 58-32 was corrected for the effects of increasing temperature based on the trend for the Barre granite.*

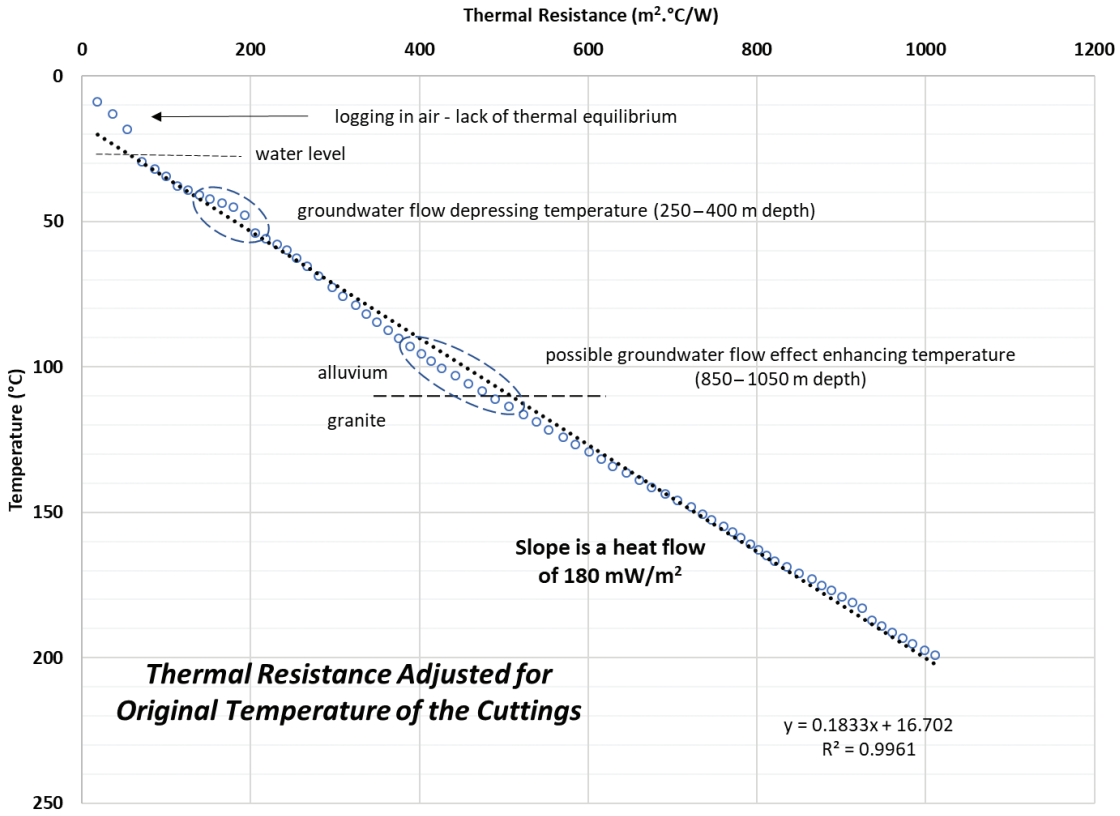

Figure 15. *Thermal resistance-temperature plot using thermal conductivities corrected for the effects of increasing temperature with depth. This reduces the heat flow from 200 mW/m² in Figure 13 to 180 mW/m².*

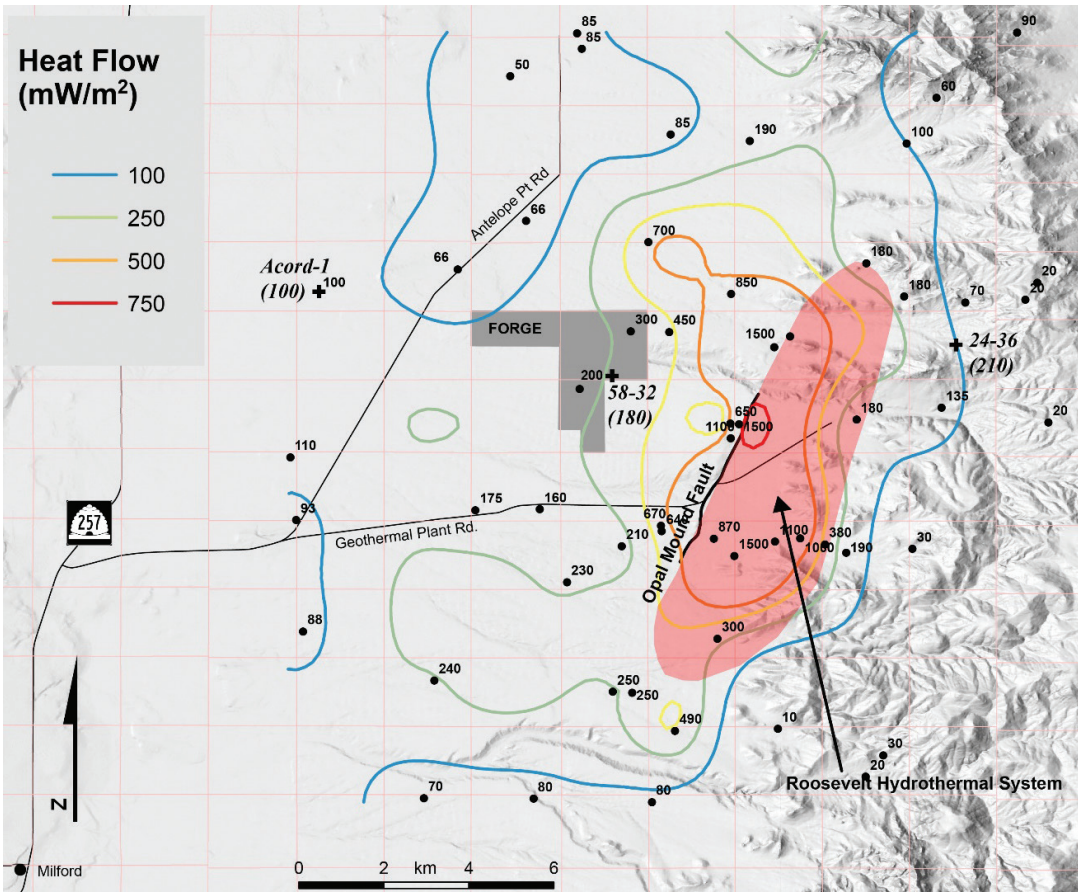

Figure 16. *Contours of conductive heat flow derived mostly from thermal gradient wells at less than 200 m depth around the Roosevelt Hot Springs hydrothermal system (mW/m²; Gwynn et al., 2016). Very high heat flows over the hydrothermal system reflect high temperature gradients overlying upflowing hot water, which at shallow depth is constrained by boiling-point-for-depth conditions. West of the hydrothermal system (that is, the OMF) the thermal regime is conductive at depth and follows a pattern of decreasing heat flow towards the west. Three wells with deep (more than 2 km) conductive thermal gradients apparently unaffected by convective or two-dimensional heat flow are marked with a cross and have their heat flow in parentheses.*

converted to heat flows using a thermal conductivity of 1.5 ± 0.3 W/m°C for the lake sediments and alluvial-fan deposits. There is a lateral flow of thermal groundwater over most of the higher heat flow areas, and shallow temperature gradients cannot be extrapolated to depth. The west edge of thermal outflow appears to be a heat flow of 100–120 mW/m^2. Integration of the shallow heat flow data yields a total heat output of the RHS system of 60–70 MW and a mass flow of 50–60 kg/s of 265°C water (Ward et al., 1978; Allis and Larsen, 2012). The area of the hydrothermal system based on wells that have responded to the pressure drawdown from the production wellfield for the power plant extends at least from well 52-21 in the south to well 12-35 about 8 km to the north, and from the OMF in the west to wells 71-10 and 14-2 almost 1–2 km to the east (Allis and Larsen, 2012; see also Figures 1 and 14). Assuming an area of the hydrothermal system of 10 to 20 km^2, the rate of heat loss is in the range of 3–7 W/m^2. This rate is over an order of magnitude larger than the deep conductive heat flow of 100–200 mW/m^2 west and east of the RHS.

Figure 17 shows isotherm maps that integrate the shallow thermal gradient well data (for example, Figure 1) with the temperature profiles in deeper wells outside of the hydrothermal system. These maps consider the contrast in thermal conductivity between basin fill and granitic rock (Gwynn et al., 2016; Hardwick et al., 2019). As discussed with Figure 1, the datum is the ground surface of the valley floor and adjacent alluvial fan, which varies from 1525 m above sea level (asl) to 1830 m asl at the western edge of the Mineral Mountains. Beneath the Mineral Mountains, the datum is fixed at 1830 m asl so that the contours are not complicated by topography. Uncertainties increase with increasing depth and with increasing distance from deep wells. In particular, the contours at 1–3 km depth beneath the Mineral Mountains may be overly conservative (too cool) because of the effects of infiltrating groundwater depressing near-surface temperatures. There is evidence for this effect in well 24-36, as discussed in the next section. The area having a temperature of more than 200°C in these maps increases from about 25 km^2 at 2 km depth, to about 70 km^2 at 3 km depth. These estimates are minimums because of the likely increase in temperature gradient with depth beneath the western flank of the Mineral Mountains.

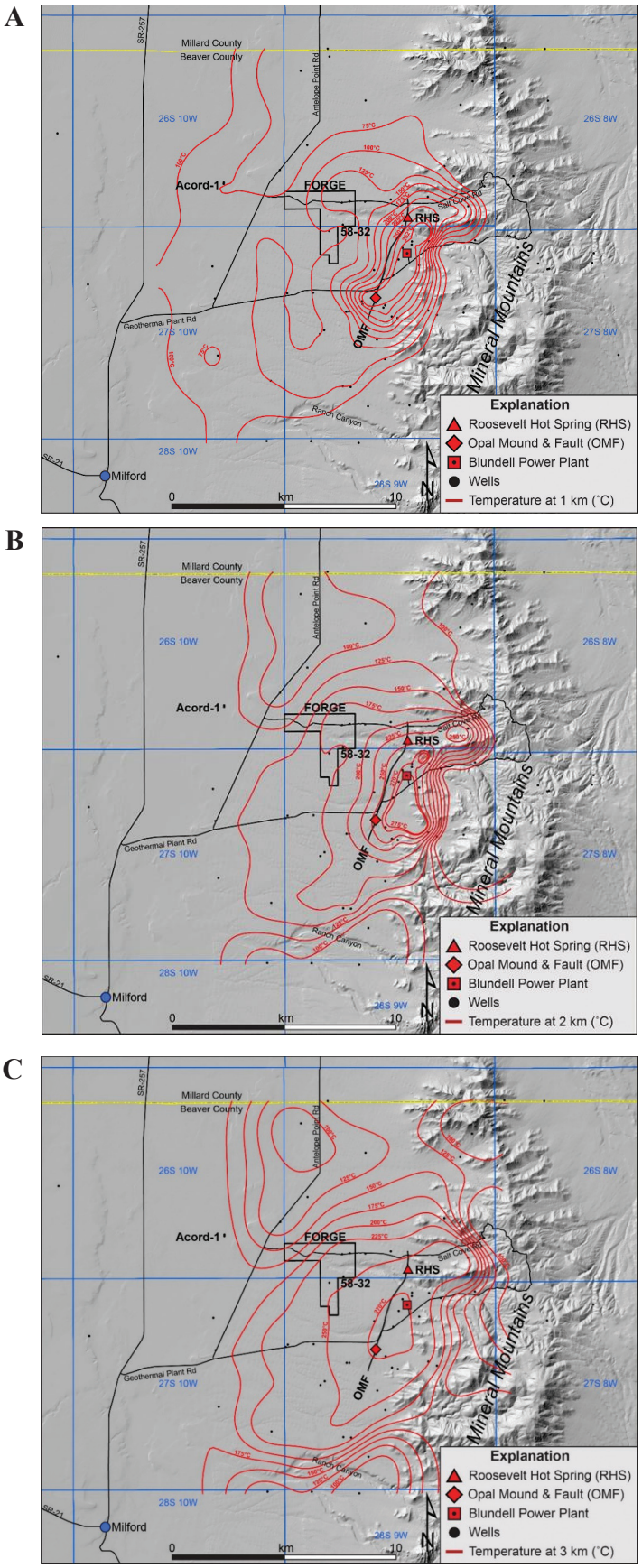

Figure 17. *Isotherm maps at* ***(A)*** *1 km,* ***(B)*** *2 km, and* ***(C)*** *3 km depth based on analysis of the temperatures in thermal gradient wells and deeper exploration wells. The datum is the ground surface beneath the valley floor and adjacent alluvial fan (1525–1830 m asl), and at 1830 m asl beneath the western flank of the Mineral Mountains.*

DEEP HEAT FLOW

Although most deep wells within the RHS system (east of the OMF) are affected by the hydrothermal upflow, at least three wells seem to be outside the upflow and their deep gradients may be indicative of the underlying conductive heat flow. These wells are Acord-1, FORGE well 58-32, and 24-36 (5 km northeast of the RHS production wells). Well 9-1, about 3 km southeast of well 58-32, could also be a candidate because it has a deep gradient of 60°C/km and is likely to have a thermal conductivity similar to 58-32 because of the similarity in granitic rocks in this well. The deep heat flow is therefore 150 mW/m^2 with an uncertainty of at least ± 20 mW/m^2. The difference in deep heat flow between 58-32 and 9-1 may not be significant given the magnitude of uncertainties, but temperatures at 1–2 km depth in 9-1 are about 50°C hotter than 58-32 due to lateral heat flow effects from the nearby hydrothermal reservoir and possibly also the hot groundwater outflow near-surface. Well 9-1 temperatures between 1 and 2 km depth are extrapolated to 3 km depth but additional extrapolation is not considered justified.

As previously discussed, a conductive geotherm fits thermal data from the ground surface to the bottom of Acord-1. The gradient in the granitic bedrock below 3 km depth is 40°C/km, and assuming an in situ thermal conductivity of 2.5 W/m°C gives a heat flow of 100 ± 20 mW/m^2 (Figure 8; Gwynn et al., 2016). FORGE well 58-32 has a conductive heat flow of 180 mW/m^2 with an estimated uncertainty of ± 20 mW/m^2. In both cases the uncertainty in heat flow is based mostly on uncertainties in thermal conductivity.

The well with the highest temperature gradient below 1 km depth on Figure 9 is 24-36, which is located near the east end of a prominent valley in the Mineral Mountains (Figure 1) and encountered granite below 90 m depth. This exploration well was unproductive and was abandoned. The temperature profile in the upper portion of 24-36 is identical to gradient well OH-7 in another valley almost 2 km to the south. OH-7 had a gradient of 48°C/km (in granite) between the surface and its total depth of 600 m. The temperature gradient in 24-36 increases to 85°C/km below 750 m depth and is constant to its total depth of 1800 m. The pattern of depressed gradients near-surface is symptomatic of the effects of downward draining of groundwater beneath the eastern flank of the Mineral Mountains. This effect is more pronounced beneath the ridgeline of the Mineral Mountains where a 600 m exploration hole had a gradient of 16°C/km (OH-3, Figure 1). Assuming an in situ thermal conductivity for the granite of 2.5 W/m°C below 750 m depth in 24-36 gives a deep heat flow of 210 ± 20 mW/m^2.

Two thermal cross sections that traverse near well 58-32 have been compiled from the thermal data. Line A–A′ extends east from Acord-1, and line B–B′ extends north from Ranch Canyon and passes 1 km east of well 58-32 (Figure 18). The south end of line B–B′ is close to a possible southern extension of the OMF. The lack of deep wells here is why the contours are dashed on Figure 18. However, the thermal gradient wells in this area show an obvious transition from thermal groundwater north of Ranch Canyon to a background gradient in three wells on the south side.

The west-east cross section highlights the relatively small area of the hydrothermal system compared to the surrounding, thermally conductive, hot rock west of the OMF, and the inferred, predominantly thermally conductive regime beneath the adjacent west flank of the Mineral Mountains at 1–3 km depth. The depth to which hydrothermal waters in the RHS have circulated is unknown, and the dip of the 300°C isotherm on either side of the upflow zone is poorly constrained. Simmons et al. (in preparation) suggest the geochemical evidence points to equilibration of the waters at a temperature of 270°–310°C. Models of high-temperature, non-magmatic geothermal systems in the Basin and Range such as Dixie Valley, Nevada, require that meteoric water circulates to between 5 and 10 km depth for a regional heat flow of 90 mW/m^2 (McKenna and Blackwell, 2004; Wisian and Blackwell, 2004; McKenna et al., 2005). These models include a steeply dipping, higher permeability fault zone which focuses the upflow of hot water between about 4 km depth and the surface.

The presence of late Quaternary rhyolite adjacent to the RHS in the Mineral Mountains (Nielson et al., 1986; Kirby et al., 2018), and geophysical evidence from seismic velocity anomalies possibly consistent with partial melt in the upper crust (Robinson and Iyer, 1981; Trow et al., 2019), could indicate a significant difference to non-magmatic fluid circulation models. Higher temperatures should be present at 5–10 km depth than occurs with a regional heat flow of 90 mW/m^2 and a non-magmatic Basin and Range setting. Becker and Blackwell (1983) modeled the fluid flow of the RHS with an initial 400°C intrusion at 5 km depth. They assumed deep circulation (9 km) and a basal heat flow of 90 mW/m^2 increasing over time to 150 mW/m^2 to sustain high temperatures at depth for several hundred thousand years. Their model required low permeability on either side of the fault zone to focus the fluid upflow in the fault zone.

Improved thermal constraints to the fluid flow in the RHS from the present study provide some additional insights. The zone of high permeability representing the fractured reservoir east of the OMF is at least 1–2 km wide and 10 km in length based on the shallow heat flow map and appears to be a broad fault zone rather than a single fault. The thermal anomaly over this fault zone at 1–2 km depth has a total heat output of 60–70 MW and is equivalent to a heat flux of at least 3–7 W/m^2 assuming a horizontal

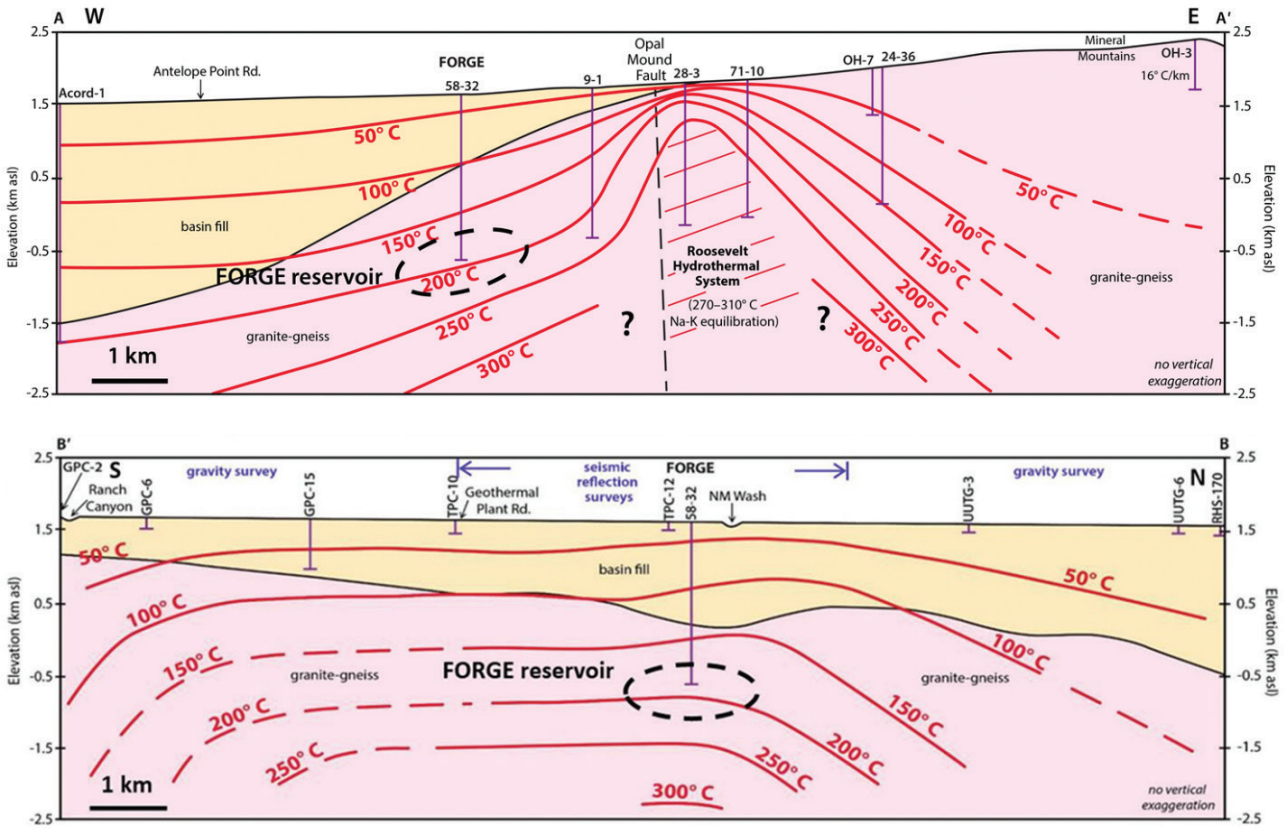

Figure 18. *Two thermal cross sections based on integration of data from many wells (locations shown on Figure 1). The contours are dashed where they are uncertain. The granite surface in B–B′ is based on preliminary interpretations from the 3-D seismic reflection survey near the FORGE site (Miller et al., 2018) and from gravity models at greater distance (Hardwick et al., 2018). Well 58-32 is 1 km east of line B–B′ and has been projected onto that line. The granite surface at that point is at 1.4 km depth, compared to 1.0 km depth in 58-32.*

area of 10–20 km^2. If the effective area of the high-permeability reservoir is less than this, the heat flux will be higher. The conductive heat flow at 2 km depth and 3 km west or east of the fault zone is about 0.2 W/m^2 and indicates a temperature of 300°C between 3 and 4 km depth. With the rate of heat extraction within the fault zone being so much greater than the high conductive heat flows on either side of the fault zone, it is likely that the rock-water equilibration temperature of 270°–310°C is much deeper than 3–4 km within the fault zone. The 300°C isotherms on Figure 18 may bend over and dip downwards as the fault zone is approached from the west or the east due to the high rate of heat mining by the hydrothermal system.

PRESSURE REGIME

At the time of the 37-day temperature profile, well 58-32 was liquid-filled with a wellhead pressure of about 7 bars gauge (0.7 MPa, 100 psi), which was bled-off so it could be logged as an open hole. The excess pressure was attributed to thermal recovery of the wellbore fluid after the injection testing. By the time of the 13-month logging there was zero wellhead pressure, and on opening, the sucking of air showed a vacuum was present above the water column. Logging showed the water level was at 90 m depth and the pressure in the open section of the well at 2300 m depth was 203 bars gauge (20.3 MPa; Figure 19). The pressure in the water column in 58-32 is very close to the pressure profiles at the same elevation in nearby groundwater wells which penetrated granite (OH4, OH5, OH1; Kirby et al., 2019). It appears that the pressure at the bottom of 58-32 may now be responding to the local (overlying) groundwater regime in the granite.

The nature of the connection between the groundwater regime and the open section of well 58-32 is unknown. The connection suggests there are fractures in the bedrock that are interconnected on a kilometer scale, although the connections are poor because of the sustained overpressure at the wellhead in the 37-day survey. However, over 12 months there has been apparent pressure equilibration. Assuming a 12-month time scale for equilibration, and a straight-line approximation to the Bower-Rice solution to the Theis equation, a transmissivity of 2 x 10^{-9} m/s is obtained. This value is right on the low end of reported permeabilities for fractured gneiss/granite (e.g., Freeze and Cherry, 1979).

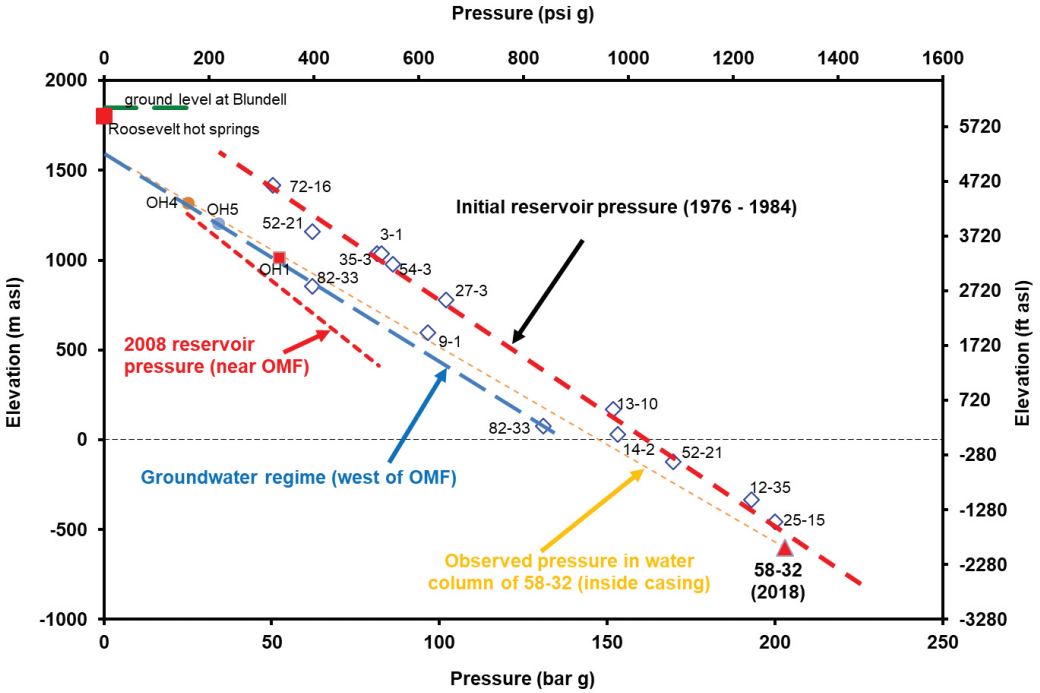

Figure 19. *Pressure trends in deep wells from the RHS reservoir east of the Opal Mound fault (OMF; modified from Allis and Larsen, 2012; 10 bars = 1 MPa), and from wells that penetrate groundwater in fractured granite west of the OMF (see Figure 1 for locations). The pressure in the open section at the bottom of well 58-32 is shown by the red triangle, and the pressure in the overlying hydrostatic column inside the casing is the dashed red line.*

CONCLUSIONS

The thermal anomaly associated with the RHS is much larger than the high-temperature upflow defined by deep productive wells drilled into the fractured granite east of the OMF. The proven zone with temperatures of more than 200°C at 1 km depth spans from well 12-15 in the south to 12-35 in the north (Figure 1), an area of at least 6 km by 2 km wide. The eastern side of this area is unconstrained due to a lack of deep wells. The shallow outflow of thermal groundwater extends at least 15 km to the north from Ranch Canyon and 10 km from east of the OMF to about Antelope Point Road. The area of hot groundwater is over ten times the area of the upflow zone. Over the southern two-thirds of this area (south of FORGE well 58-32), the temperature at the water table is lower than the outflow plume to the north (typically less than 50°C west of the OMF) and there is no evidence of a temperature inversion at greater depth (Figure 4). The temperature gradient in the alluvium-hosted groundwater here is about 70°C/km which is consistent with an underlying conductive heat flow of about 100 mW/m^2. The lack of a temperature inversion also means the thermal outflow here is relatively thin and near the water table, similar to the scenarios modeled by Ziagos and Blackwell (1981, 1986), and this outflow has persisted for at least several tens of thousands of years. The numerous patches of siliceous sinter adjacent to the OMF including the Opal Mound may have built up during periods of higher pressure in the evolution of the RHS system, such as would have occurred during the highstand of Lake Bonneville 18,000 years ago.

The northern sector of the shallow thermal regime is dominated by a high-temperature outflow plume best illustrated in well OH-5 (Figure 5), and originally recognized by Ward et al. (1978) and Wilson and Chapman (1980). The peak temperature is at about 300 m depth, and it has a temperature of at least 130°C (well 82-33) northwest of the OMF, and possibly over 200°C if well 12-35 is near where the plume exits from the upflow zone. The presence of a strong temperature inversion beneath the center of the outflow plume (OH5) shows that this is a relatively recent feature (~ 100–1000 years).

Detailed temperature and thermal conductivity measurements in FORGE well 58-32 reveal a predominantly conductive thermal profile with a heat flow of 180 ± 20 mW/m^2 when thermal conductivity is corrected for in situ temperature. The temperature at the bottom of the well (2300 m) is 199.4°C. The temperature gradient in the well varies between 60° and 90°C/km depending on bedrock thermal conductivity. Near the bottom of the well in predominantly granite the gradient is close to 70°C/km. A thermal resistance plot shows evidence of a lateral flow of groundwater outside the casing between 250 and 400 m depth. There also appears to be slightly elevated temperatures centered near the alluvium/bedrock interface which may indicate lateral flow at that depth as well.

Prior to development of geothermal power, the highest-temperature and most productive area of the reservoir had wells with boiling-point-for-depth temperature profiles from near-surface to about 400 m depth where the temperature was above about 250°C, and wells had very low thermal gradients at greater depth. The boiling point profile is typical for an upflow zone of a hydrothermal system. Outside of the productive area, all but one deep well (12-35) have conductive thermal gradients below about 1 km depth. For some of the deep wells such as 52-21 and 82-33, only one thermal profile is available, and there is uncertainty over how close to thermal equilibrium it is. The inferred deep thermal gradients in these two wells therefore also have greater uncertainty. Despite the uncertainties, the volume of the high-temperature reservoir appears to be small compared to the volume of rock having vertically extensive conductive thermal gradients. The large volume of inferred low-permeability rock highlights the need to develop technologies that can fracture the rock and greatly increase the electric power potential.

Despite the large volume of apparently thermally conductive rock around the main high-temperature upflow zone, wells within a zone about 2 km wide east of the OMF have responded rapidly to pressure drawdown from the production wellfield (Allis and Larsen, 2012). This drawdown area ranges from the southernmost deep exploration well (52-21) to the northernmost deep well (12-35), and in Figure 14 this area is referred to as the "hydrothermal system." The wells in the system had the same pressure profiles prior to development suggesting good communication with the high-temperature upflow zone. Clearly at least one fracture at some depth in each well connects to the upflow and controls the pressure regime in the well, even though the bulk of the host rock may be impermeable. The OMF itself may also be a zone of lateral and vertical permeability which allows subsurface outflow of cooler geothermal water (40°C) from the hydrothermal system into the regional groundwater as far south as Ranch Canyon (Figure 1). The permeability pattern of a relatively localized high-temperature upflow zone, surrounded by a complicated, dispersed pattern of secondary fracturing, is similar to the generalized geothermal model for Basin and Range systems described by Blackwell et al. (2012).

The uniform conductive thermal regime below 1 km depth in several of the wells outside of the hydrothermal zone may be extrapolated to much greater depth. There is diverse evidence for partial melt deeper in the crust from a low-velocity and attenuation anomaly (Robinson and Iyer, 1981; see also Trow et al., 2019), and helium anomalies (Simmons et al., in preparation). Figure 20 shows the extrapolated profiles in wells Acord-1, 58-32 and 24-36 assuming constant, one-dimensional heat flow with thermal conductivity only varying with temperature as shown in Figure 14. The effects of heat production from uranium, thorium, and potassium in the granite measured at the FORGE site have a very small effect on the extrapolated temperatures and have been ignored. Temperatures of about 600° to 700°C, often associated with the initiation of partial melting in wet granitic rocks, occur between 6 and 8 km depth beneath wells 58-32 and 24-36, and at 10–12 km in Acord-1. The 6–8 km depth is the same as a transition to lower seismic velocity inferred from recent ambient noise tomographic surveys (Trow et al., 2019). Lower heat flow in Acord-1 indicates possible melting at much greater depth in the center of north Milford Valley. There is no thermal data constraining the eastern side of the partial melt zone inferred from 24-36. The partial melt zone could extend to beneath the adjacent ridge of the Mineral Mountains where rhyolite has been extensively extruded over the last 1 million years.

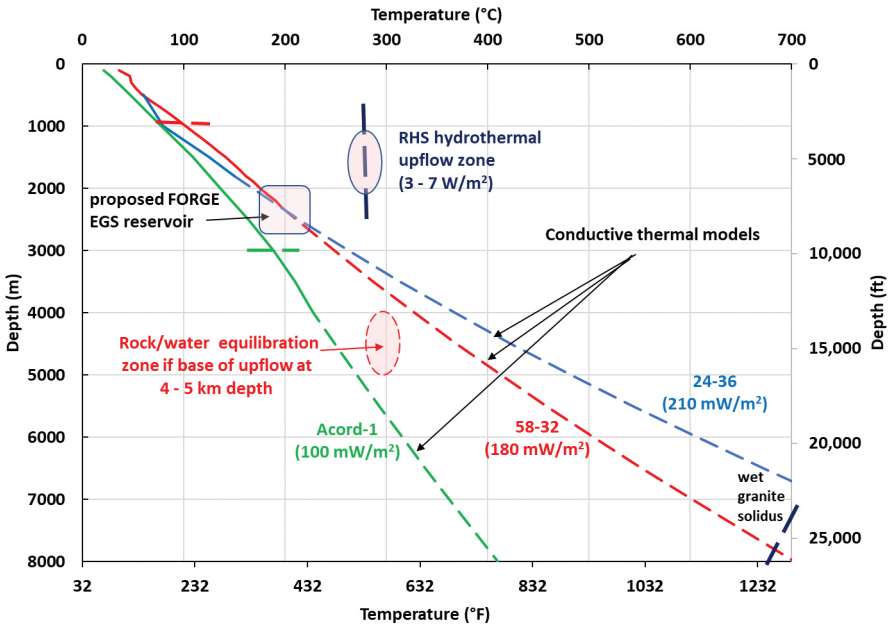

Figure 20. *Extrapolated geotherms for three wells outside the RHS hydrothermal system Thermal models assume constant, one-dimensional heat flow based on the observed thermal gradient and thermal conductivity below 1 km depth. The average thermal conductivity was assumed to be 2.5 W/m°C at 200°C in granite, and conductivity decreased with temperature based on the trends in Figure 14.*

Figure 20 also shows that if water in the RHS hydrothermal system is circulating to at least 4–5 km and this is where the 270°–310°C rock-water equilibrium chemistry is established, then the temperature at that depth could be 100°C lower than the at same depth on either side where thermally conductive conditions are the dominant form of heat loss. This is not surprising because the convective heat loss from the hydrothermal system is over an order of magnitude greater, causing more intense heat mining at depth.

ACKNOWLEDGMENTS

This worked was funded by the Geothermal Technologies Office of the U.S. Department of Energy, and by the Utah Geological Survey. PacifiCorp provided access to historical documents and well data related to the exploration of the RHS. Di Drill Survey Services ran the temperature profile in 58-32. The manuscript has benefited from discussion with Stefan Kirby and Stuart Simmons, and reviews by David Chapman, Maria Richards, Stephanie Carney, and Mike Hylland.

REFERENCES

Allis, R.G., Nash, G.D., Johnson, S.D., 1999, Conversion of thermal infrared surveys to heat flow—comparisons from Dixie valley, Nevada, and Wairakei, New Zealand: Transactions, Geothermal Resources Council, v. 23, p. 499–504.

Allis R.G. and Larsen, G., 2012, Roosevelt Hot Springs geothermal field, Utah—reservoir response after more than 25 years of power production: Proceedings, 37th Workshop on Geothermal Reservoir Engineering, Stanford University, Stanford, CA, 8 p.

Allis, R.G., Gwynn, M., Hardwick, C., Kirby, S., Moore, J., and Chapman, D., 2015, Re-evaluation of the pre-development thermal regime of Roosevelt Hot Springs geothermal system, Utah: Proceedings, 40th Workshop on Geothermal Reservoir Engineering, Stanford University, Stanford, CA., 12 p.

Allis, R., Gwynn, M., Hardwick, C., and Moore, J., 2018, The challenge of correcting bottom-hole temperatures—An example from FORGE 58-32, near Milford, Utah: Proceedings, 43rd Workshop on Geothermal Reservoir Engineering, Stanford University, Stanford, CA, 8 p.

Becker, D.J., and Blackwell, D.D., 1983, Gravity and hydrothermal modeling of the Roosevelt Hot Springs area, southwestern Utah: Journal of Geophysical Research, v. 98, B10, p. 17,787–17,800.

Blackwell, D.D., Waibel, A.F., and Richards, M., 2012, Why Basin and Range systems are hard to find—the moral of the story is they get smaller with depth!: Transactions, Geothermal Resources Council, v. 36, p. 1321–1326.

Bromley, C.J., Van Manen S.K., and Mannington, W., 2011, Heat flux from steaming ground—reducing uncertainties: Proceedings, 36th Workshop on Geothermal Reservoir Engineering, Stanford University, Stanford, CA, 7 p.

Bullard, E.C., 1939, Heat flow in South Africa: Proceedings of the Royal Society of London, Series A, v. 173, p. 474–502.

Capuano, R.M., and Cole, D.R., 1982, Fluid-mineral equilibria in a hydrothermal system: Geochimica Cosmochimica Acta, v. 46, p. 1353–1364.

Faulder, D.D., 1991, Conceptual geologic model and native state of the Roosevelt Hot Springs hydrothermal system: Proceedings, 16th Workshop on Geothermal Reservoir Engineering, Stanford University, p. 131–142.

Faulder, D.D., 1994, Long-term flow test #1, Roosevelt Hot Springs, Utah: Transactions, Geothermal Resources Council, v. 18, p. 583–590.

Forrest, R.J., 1994, Geothermal development at Roosevelt Hot Springs geothermal area Beaver County, Utah, 1972–1993: Utah Geological Association, 23, p. 37–44.

Freeze, R.A. and Cherry, J.A., 1979, Groundwater: New Jersey, Prentice-Hall Inc, 604 p.

Gwynn, M., Allis, R., Hardwick, C., Hill, J., and Moore, J., 2016, A new look at the thermal regime around Roosevelt Hot Springs, Utah: Transactions, Geothermal Resources Council, v. 40, p. 551–558.

Gwynn, M., Allis, R., Hardwick, C., Jones, C., Nielsen, P., and Hurlbut, W., 2019, Compilation of rock properties from FORGE well 58-32, Milford, Utah, *in* Allis, R., and Moore, J.N., editors, Geothermal characteristics of the Roosevelt Hot Springs system and adjacent FORGE EGS site, Milford, Utah: Utah Geological Survey Miscellaneous Publication 169-L, 36 p., https://doi.org/10.34191/MP-169-L.

Hardwick, C., Hurlbut, W., and Gwynn, M., Allis, R., Wannamaker, P., and Moore, J., 2018, Geophysical surveys of the Milford, Utah, FORGE site—gravity and TEM: Transactions, Geothermal Resources Council, v. 42, p. 1071–1083.

Harrison, M.T., Morgan, P., and Blackwell, D.D., 1986, Constraints of the age of heating at the Fenton Hill site, Valles Caldera, New Mexico: Journal of Geophysical Research, v. 91, no. B2, p. 1899–1908.

Jones, C.G., Moore, J.N., and Simmons, S., 2019, Petrography of the Utah FORGE site and environs, Beaver County, Utah, *in* Allis, R., and Moore, J.N., editors, Geothermal characteristics of the Roosevelt Hot Springs system and adjacent FORGE EGS site, Milford, Utah: Utah Geological Survey Miscellaneous Publication 169-K, 23 p., 2 appendices, https://doi.org/10.34191/MP-169-K.

Kirby, S.M., Knudsen, T., Kleber, E., and Hiscock, A., 2018, Geologic setting of the Utah FORGE site based on new and revised geologic mapping: Transactions, Geothermal Resources Council, v. 42, p. 1097–1114.

Kirby, S.M., Simmons, S., Inkenbrandt, P.C., and Smith, S., 2019, Groundwater hydrogeology and geochemistry of the Utah FORGE site and vicinity, *in* Allis, R., and Moore, J.N., editors, Geothermal characteristics of the Roosevelt Hot Springs system and adjacent FORGE EGS site, Milford, Utah: Utah Geological Survey Miscellaneous Publication 169-E, 21 p., https://doi.org/10.34191/MP-169-E.

Lee, W.T., 1908, Water resources of Beaver Valley, Utah: U.S. Geological Survey Water-Supply Paper no. 217, 55 p.

Lynne, B.Y., Campbell, K.A., Moore, J.N., and Browne, P.R.L., 2005, Diagenesis of 1900-year-old siliceous sinter (opal-A to quartz) at Opal Mound, Roosevelt Hot Springs, Utah: Sedimentary Geology, v. 179, no. 3-4, p. 249–278.

McKenna, J.R., and Blackwell, D.D., 2004, Numerical modeling of transient Basin and Range extensional geothermal systems: Geothermics, v. 33, p. 457–476.

McKenna, J.R., Blackwell, D.D., and Richards, M.C. and Swenson, D.V., 2005, Natural state modeling, structure, preliminary temperature and chemical synthesis of the Dixie Valley, Nevada geothermal field: Proceedings, 30th Workshop on Geothermal Reservoir Engineering, Stanford University, 8 p.

Miller, J., Allis, R. and Hardwick, C., 2018, Seismic reflection profiling at the FORGE, Utah EGS site: Transactions, Geothermal Resources Council, v. 42, p. 1115–1127.

Moore, J., McLennan, J., Allis, R., Pankow, K., Simmons, S., Podgorney, R., Wannamaker, P. and Rickard, B., 2018, The Utah Frontier Observatory for Geothermal Research (FORGE)—Results of Recent Drilling and Geoscientific Surveys: Transactions, Geothermal Resources Council, v. 42, p. 1128–1137.

Mundorff, J.C., 1970, Major thermal springs of Utah: Utah Geological Survey Water Resources Bulletin 14, 60 p.

Nielson, D.L., Evans, S.H., and Sibbett, B.S., 1986, Magmatic, structural, and hydrothermal evolution of the Mineral Mountains intrusive complex, Utah: Geological Society of America Bulletin, v. 97, p. 765–777.

Robertson, E., 1988, Thermal properties of rocks: U.S. Geological Survey Open File Report 88-441, 106 p.

Robinson, R. and Iyer, H.M., 1981, Delineation of a low-velocity body under the Roosevelt Hot Springs geothermal area, Utah—Using teleseismic p-wave data: Geophysics, v. 46, p. 1456–1466.

Sibbett, B.S. and Nielson, D.L., 2017, Geologic map of the central Mineral Mountains (GIS of 1980 map), Beaver County, Utah: Utah Geological Survey Miscellaneous Publication, 17-2DM.

Simmons, S.F., Kirby, S., Moore, J.N., Wannamaker, P., and Allis, R., 2015, Comparative analysis of fluid chemistry from Cove Fort, Roosevelt and Thermo—Implications for geothermal resources and hydrothermal systems on the east edge of the Great Basin: Proceedings Geothermal Resources Council, v. 39, p. 55–61.

Simmons S., Kirby, S., Allis, R., Moore, J., and Fischer, T., 2018, Update on production chemistry at Roosevelt Hot Springs, Utah: Proceedings, 43rd Workshop on Geothermal Reservoir Engineering, Stanford University, Stanford, CA, 7 p.

Simmons, S., Allis, R., Kirby, S., Moore, J., and Fisher, T., in prep., The origin and evolution of hydrothermal fluids and their flow in response to >30 years of geothermal production, Roosevelt Hot Springs, Utah, USA: manuscript not yet submitted.

Trow, A.J., Pankow, K.L., Wang, Y., and Lin, F.-C., 2019, Localized ambient noise tomography over the FORGE Utah site, *in* Allis, R., and Moore, J.N., editors, Geothermal characteristics of the Roosevelt Hot Springs system and adjacent FORGE EGS site, Milford, Utah: Utah Geological Survey Miscellaneous Publication 169-J, 15 p., https://doi.org/10.34191/MP-169-J.

Ward, S.H., Parry, W.R., Nash, W.P., Sill, W.R., Cook, K.L., Smith, R.B., Chapman, D.S., Brown, F.H., Whelan, J.A., and Bowman, J.R., 1978, A summary of the geology, geochemistry, and geophysics of the Roosevelt Hot Springs thermal area, Utah: Geophysics, v. 43, p. 1515–1542.

Wilson, W.R., and Chapman, D.S., 1980, Thermal studies at Roosevelt Hot Springs, Utah: unpublished report prepared by Department of Geology and Geophysics, University of Utah, Salt Lake City, Utah, for U.S. Department of Energy, Division of Geothermal Energy, 102 p., http://www.osti.gov/scitech/biblio/7015581.

Wisian, K., and Blackwell, D.D. 2004, Numerical modeling of Basin and Range geothermal systems: Geothermics, v. 33, p. 173–741.

Ziagos, J., and Blackwell, D., 1981, A model for the effect of horizontal fluid flow in a thin aquifer on temperature-depth profiles: Transactions, Geothermal Resources Council, v. 5, p. 221–223.

Ziagos J., and Blackwell D., 1986, A model for the transient temperature effects of horizontal fluid flow in geothermal systems: Journal of Volcanology and Geothermal Research, v. 27, no. 3-4, p. 371–397.